Assessment of local outburst flood risk from successive landslides: case study of Baige landslide-dammed lake, upper Jinsha river, eastern Tibet

Dingzhu Liu[1,3], Yifei Cui[2*], Hao Wang[4], Wen Jin[1,3], Chunhao Wu[1,3], Nazir Ahmed Bazai[1,3], Guotao Zhang[1,3], Paul A. Carling[5], Huayong Chen[1]

[1] Key Laboratory of Mountain Hazards and Earth Surface Process/Institute of Mountain Hazards and Environment, Chinese Academy of Sciences, Chengdu, China

[2] State Key Laboratory of Hydroscience and Engineering, Tsinghua University, Beijing 100084, China

[3] University of Chinese Academy of Sciences, Beijing, China

[4] Key Laboratory of Land Surface Pattern and Simulation, Institute of Geographic Sciences and Natural Resources Research,CAS, Beijing,100101, China

[5] Geography and Environment, University of Southampton, Southampton, United Kingdom

[*] Corresponding Author: yifeicui@mail.tsinghua.edu.cn

Abstract

Two large landslides in October and November 2018 sequentially dammed the Jinsha river at Baige village, eastern Tibet, China. Subsequently, breaching of each dam induced massive outburst floods that posed a severe threat to downstream cities and infrastructure. Field investigation indicates volumes of the first and second landslide dam are about 24.5×10^6 m^3 and 8.53×10^6 m^3, respectively. However, the peak discharge of the flood generated from the second landslide (3.1×10^4 m^3/s) was significantly larger than that from the first (1.0×10^4 m^3/s). The second peak discharge would have been 5.15×10^4 m^3/s if the dam breached naturally. In this study, we developed two geometry parameters: effective dam height H_e (elevation difference between overtopping level and river bottom) and a narrowing number distribution $N_r(H)$ (measures the

degree to which a river section is occupied by landslide materials to elevation H) which represents river section narrowing effects of successive landslides. Using numerical simulations, we show that H_e dominates peak discharge, and it has a linear relationship with peak discharge with slope of 1009.4 m^2/s. Furthermore, the dam includes two sub-areas: a higher part (SB-1) and a lower part (SB-2). Two floods only eroded SB-2. However, breaching of SB-1 and breached SB-2 still narrowed the river. The narrowing effects of the first and second breached dam on the river channel are around 0.35 and 0.5, respectively. Spillway and landslide runup deposits increased the local flood risk by narrowing and lifting the local river section; the first landslide promoted the second landslide, which occupied the same area and forms a dam with high H_e value. Consequently, a more catastrophic flood could be triggered by a small subsequent landslide. Spatial superposition of successive landslides increased the local flood risk. This research quantitatively analyzed the influence of the geometry of dam induced by successive landslides on the process of outburst floods and the risk.

Key words: Successive landslides, Successive outburst floods, Multi-hazard chain, Effective dam height, Narrowing effect.

1 Introduction

Mountain areas are susceptible to landslides triggered by rainfall and earthquakes (Wang et al., 2008; Cui et al., 2012; Zhang et al., 2019; Yan et al., 2020). Some of these landslides block rivers and form earthen landslide dams that impound barrier lakes. Lake development leads to back-flooding upstream and may inundate roads and villages. Most barrier lake dams breach a short time after formation, causing impounded water to be released in an outburst flood (Costa and Schuster,

1988; Cui et al., 2012; Bazai, et al., 2021). Outburst floods are some of the most catastrophic hazards on Earth and pose a great threat to people and infrastructure downstream (Cui et al., 2009; Bazai, et al., 2021). Outburst floods may also have significant geomorphic and geologic impacts; they have huge erosive and sediment transport capacity that can rapidly transform river channels and bedforms (Carling, 2013; Turzewski et al., 2019; Carling and Fan, 2020), and may lead to climate change (Teller et al., 2002) and global sea level change (Garcia et al., 2009). Outburst floods and their impacts appear in the myths and stories of many civilizations. (Burr et al., 2009).

In nature, landslide dams fail due to overtopping, piping and slope failure, with overtopping the most common failure type (Costa and Schuster, 1988). There are several stages to the overtopping process; the most powerful outburst flood discharge forms after the retrogressive stage (Walder et al., 2015; Jiang et al., 2018), resulting in strong vertical and horizontal erosion of the dam and the downstream transport of much of the dam material. During this stage, vertical and horizontal erosion of the dam tends to develop at the same pace to form a trapezoidal spillway (Niu et al., 2012; Al-Riffai, 2014; Walder et al., 2015). Peak discharge is the most important parameter in terms of outburst flood risk (Cui et al., 2012), and it may be influenced by many factors including dam geometry, soil physical properties, upstream valley geometry, volume of barrier lake, etc. (Peng, 2012). Peak discharge has been found to have the highest correlation with lake volume (Peng, 2012).

Many methods are available for peak discharge calculation, including empirical and numerical simulation models using zero-, one-, two- and three-dimension formulations. Empirical methods are widely used, but the models are implemented post hoc usually employing data collected after the event and cannot capture the discharge curve and dam deformation (Costa and Schuster, 1988; Cui

et al., 2012; Peng, 2012). However, numerical methods, based on physical principles of hydrodynamics and erosion, allow modeling of outburst flood hydrograph and spillway evolution (Fread, 1988; Begam et al., 2018). For zero dimension models, flow is considered as a broad weir and discharge is calculated from weir flow formulae (Fread, 1988; Chang and Zhang, 2010; Singh, 2013; Chen et al., 2014), a simple and reliable method (Walder et al., 2015). More detailed numerical simulation is based on morpho-dynamic models, using the Navier-Stokes equations or their depth-averaged forms (1D or 2D shallow water equations) to calculate flood hydrodynamics and erosion and deposition models to predict bedform change (Wang et al, 2008; Cao et al., 2011; Swartenbroekx et al., 2013; Bohorquez et al., 2019). Generally, erosion is calculated through river dynamic models (such as the Meyer-Peter and Müller model, Duboys model, Einstein-Brown model, etc.) in most simulations. However, Chen et al., (2014) proposed that non-linear hyperbolic erosion models produce more accurate results compared with natural dam breach observations (Chen et al., 2014; Zhou, 2015).

Previous studies of outburst flood risk have focused on single river blocking events, but successive river blocking events have not been considered even though many have been reported. Examples of successive blocking mechanisms include glacier avalanche (Capps and Clague, 2014; Cook et al., 2016), ice-avalanche (Chen et al., 2020), debris flow (Wei et al. 2018; Hu et al., 2019) and landslide (Li et al., 2016; Fan et al., 2019b; Liu et al., 2019). These local successive river blocking events often lead to successive outburst floods. In eastern Tibet, the Parlung Zangbo river has been blocked by debris flows from Tianmo gully many times (Wei et al., 2018); Yigong lake was blocked by catastrophic landslides in 1902 and 2000 (Zhou et al., 2016) and formed outburst

floods with peak discharges of around 18.9×10^4 m^3/s (Ma, 2006) and 12.4×10^4 m^3/s (Liu et al., 2019), respectively; the Yarlung Tsangpo gorge was blocked twice in 2018, with a peak discharge of 3.2×10^4 m^3/s in the second outburst flood (Hu et al., 2019; Chen et al., 2020).

Statistical analysis by Samia et al. (2017) suggests a 60% chance of landslide source areas generating a second event within 10 years of the first; the initial blocking event would influence the impact of the next event on local river geometry. Some landslide dams, failed and intact, remain in the river for a substantial time(Schuster, 2006) and may have a profound effect on watershed geomorphic evolution, especially if they function as knickpoints (Korup et al., 2006; Owen, 2008). Knickpoint evolution moderates the channel blocking process (Korup and Montgomery, 2008), with the remnant lake and spillway influencing the river longitudinal profile and watershed vertical evolution (Wang et al., 2019). Spillways may be eroded by base flow, seasonal floods or outburst floods (Choi et al. 2018). Furthermore, retrogressive river erosion can be inhibited where rivers are blocked long term by dams and barrier lakes have formed (Korup and Montgomery, 2008), whereas outburst floods flush out sediment, including boulders, and may even change river geometry (Carling, 2013; Lang et al., 2013; Larsen and Lamb, 2016; Liu et al., 2019). River blocking impacts also include lateral narrowing and longitudinal lifting of the river, but few studies focus on river narrowing and analysis of successive landslides is still at an early stage (Liao et al., 2019). In the present study, we focus on the geometric parameters of landslide dams that influence the dam breach event, using the case study of landslides at Baige, on the Jinsha river in eastern Tibet, in order to better understand the role of successive landslides on local outburst flooding.

2 Successive Baige landslides and outburst floods, 2018

The study landslides originated close to the village of Baige, to the west of Jinsha river in Jiangda county; Tibet (98°42′17.98″ E, 31°4′56.41″N) (Ouyang et al., 2019); the river forms the boundary between Sichuan and Tibet in this area. The Jinsha river follows the suture zone between the Changdu-Simao Block (in Tibet) and the Chuan-Dian Block (in Sichuan Province), with the main base rocks comprising gneiss, ophiolite and carbonaceous slate. Prior to the landslide events, the river bed elevation was around 2870 m and the average river width was about 93 m.

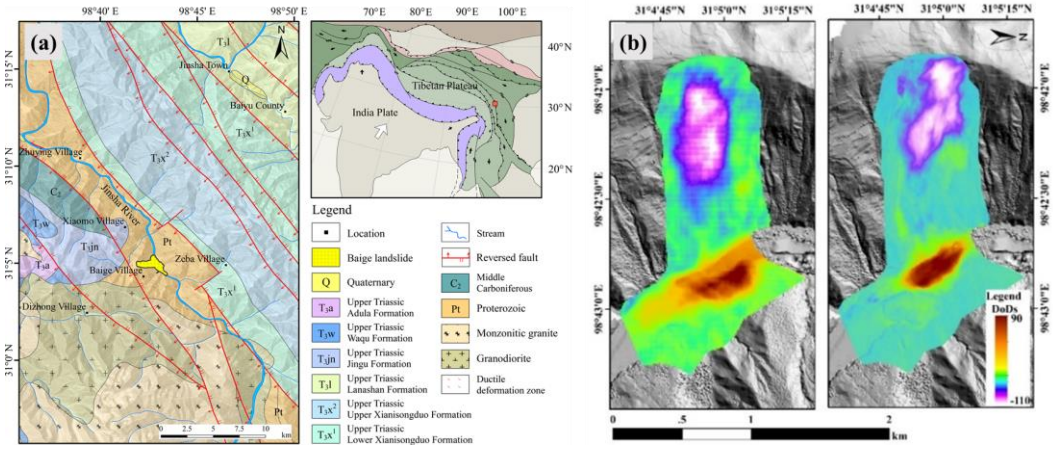

Fig. 1. Location context: (a) Geological context of Baige landslides; (b) DEMS of difference (DoDs) showing elevation change following the first (left) and second (right) landslide.

The first landslide occurred at 22:06 h on October 10, 2018. The area of the slide had an altitudinal range of about 850 m and a slide distance of 1400 m, giving an area of 5.26×10^5 m^2. The landslide flowed at high speed, blocked the Jinsha river and formed a landslide dam of 46 m average height and total volume of 24.5×10^6 m^3. The dam was more than 2 km in length in a downstream direction and had an average width of 450 m along the river. Landslide run up on the opposite side of the Jinsha canyon was 160 m. At 15:30 h on October 12, a natural spillway started

to form on the right side of the dam, although the water level of the impounded lake continued to rise until 00:45 h on October 13, with a maximum elevation of 2933.7 m and volume of 2.9×10^8 m^3. By 8:00 h on October 13, the lake water level had decreased by 20.3 m with a lake volume of 1.8×10^8 m^3, after 18 hours, eventually, the lake water level decreased to around 2893 m and the dam breach stopped. Peak discharge of the dam breach occurred at 7:00 h on October 13 at 1×10^4 m^3/s. A peak discharge of 7800 m^3/s was recorded at Yebatan electricity station, located 70 km downstream. The dam breach formed a trapezoidal-shaped spillway with a basal width of 60 m and top width of 200 m, and 4.0×10^6 m^3 of sediment was transported downstream.

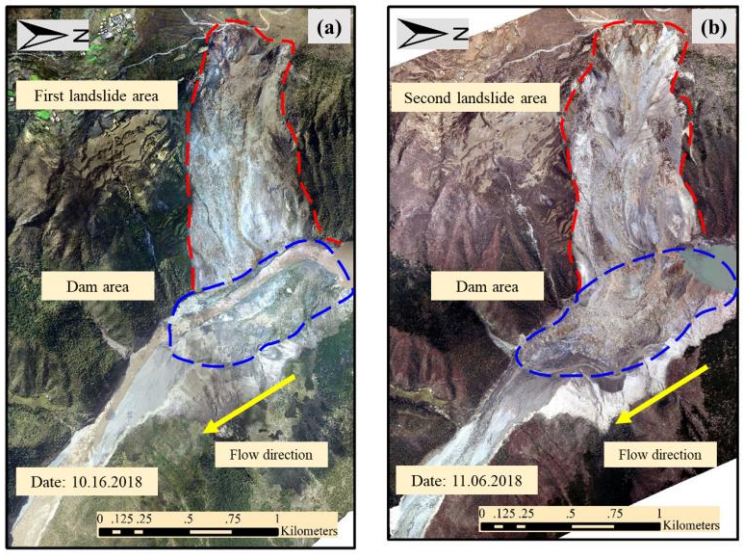

Fig. 2. Plan view aerial drone images: (a) after first dam breach; (b) after second dam breach

The second landslide occurred at 17:40 h on November 3, 2018 and blocked the Jinsha river around the location of the spillway eroded by the first outburst flood, which was still filled with landslide debris. The main scarp of the landslide was at an elevation of 3720 m and the landslide had a volume of 8.5×10^6 m^3. The new dam had a maximum length of 2.1 km in a downstream direction and maximum and average widths of 700 m and 450 m, respectively. The surface elevation

of the dam varied from 2966 m to 3011 m. Due to the high risk of a second dam break, emergency spillway excavation was conducted to decrease the risk. The basal elevation of the excavated spillway was 2952.5 m, with a side slope of 1:3 (height:width), basal width of 3 m and length of 350 m. The excavation was finished at 09:00 h on November 12. The dam started to breach at 10:50 h on November 12. During the retrogressive stage, at 15:00 h on November 13, a total of 1.32×10^6 m^3 of dam sediment was transported downstream, increasing to 1.59×10^6 m^3 by 16:00 h. An outburst flood peak discharge of 3.1×10^4 m^3/s was recorded at 18:00 h on November 13. The water level of the outburst flood flow downstream was greater than the 10000-year flood and it caused catastrophic damage to downstream settlements and regions, including the destruction of bridges, tourist spots and farmland. A balance between lake inflow and discharge was reached at 8:00 h on November 15 2018, with an upstream lake volume of 7.9×10^7 m^3. All these data for two events are represented in Table 1.

Table1 Summary geometry data for the two 2018 Baige landslide dams

Case	L_D (m)	B_D (m)	h_{avg} (m)	V_D (10^6 m^3)	h_T / V_{ML}($\times10^8$ m^3)	H_s (m)
First dam	2100	500	40	24.5	2933.7/2.9	2892.84
Second dam	2100	700	46	8.53	2956.39/5.86	2903.81

Compared with the lake volume before the dam breach, the landslide material only comprises a small part of the initial lake volume. The first dam breach left 13.56% of the volume of the initial lake, while the second dam breach left 13.61% of the volume of the second initial lake as residual storage; lake depth upstream of the spillway is 33.8 m.

Costa and Schuster (1988) classified landslide dams into six categories based on their depositional form, sliding mechanism and spatial relationships with the valley floor. Baige events blocked the Jinsha river totally in both cases, and are classified as Type 2 as the dams are large and

span the entire river.

3 Methods

3.1 Field investigation and Digital Elevation Model (DEM) analysis

For comparison of dam geometry evolution, field investigation was carried out six months after the second Baige dam breach. A small unmanned aerial vehicle (UAV), Dajiang MAVIC 2, was used to obtain multiple aerial photographs using a high-resolution (4000 × 2250) camera. All the images exhibit minimum 80% image overlap. (Tonkin and Midgley, 2016; Entwistle and Heritage, 2017; Entwistle and Heritage, 2019). The drone was flown at a uniform height (300 m) to generate high-resolution imagery (0.1 m, vertically and horizontally) for accurate Digital Terrain Modelling (DTM) reconstruction. We obtained ground truth data using RTK (Real-Time Kinematic) Global Positioning System (GPS) technology to determine altitude and the location of 20+ markers on each landslide dam. The DEM data used to analysis geometric characteristics range in resolution from 10 m (pre-landslide), 1 m (post-first landslide, post-first dam breach and post second landslide) to 0.5 m (post-second dam breach).

DEM differencing has been used to analyze the volume and elevation variations between time periods. Morphological change is determined using DoD:

$$\Delta E = E_2 - E_1 \quad (1)$$

where ΔE is the elevation difference in one mesh, m, E_1 and E_2 are the elevations at specific times, such as after one event.

3.2 Dam breach numerical simulation

The overtopping process of the outburst flood was modeled as open channel flow and a weir flow model was used to predict the flow rate in the spillway (Chen et al., 2014; Walder et al., 2015). Many erosion models have been developed to predict flow erosion, and they can be generally grouped into three categories: (1) river dynamic models based on sediment entrainment and transportation that can be used with the Exner equations to update geometry variation (Wang et al., 2008; Cao et al., 2011; Begam et al., 2018); (2) models based on soil mechanics (Briaud et al., 2001; Hanson and Simon, 2001; Chang et al., 2011; Zhong et al., 2020); (3) empirical erosion models based on observations of natural dam breach processes, but verified in physical experiments (Chen et al., 2014; Wang et al., 2016). The composition of natural dams is complex, including inner and outer structure, varying lithology, particle size gradation and water content, etc. Flow erosion is influenced by the soil mechanics and sediment properties simultaneously, so that the dam breach erosion process is very complicated. Here, we adopted the Broad-Crested Weir Flow model of Chen et al. (2014) and related erosion model to analysis the dam breach (Fig. 3).

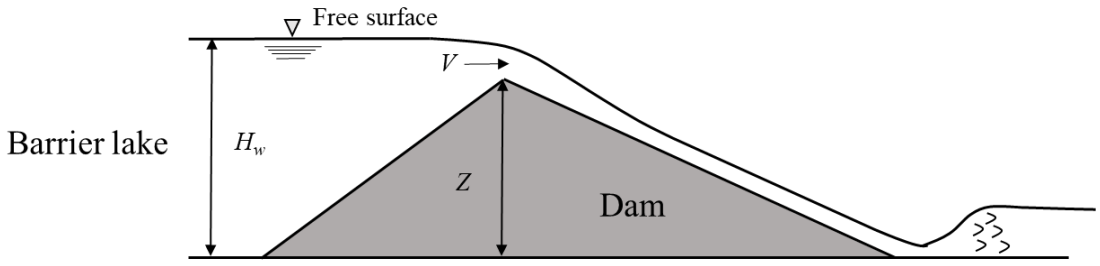

Fig. 3. Cross section showing dam breach parameters

$$Q = CB_c\sqrt{2g}(H-Z)^{\frac{3}{2}} = A(H)\frac{\Delta H}{\Delta t} + q \quad (2)$$

where Q is spillway discharge; C is a discharge coefficient; B_c is the average width of the spillway;

Z is the elevation of the spillway base; H is the elevation of the spillway water surface; g is the acceleration due to gravity (9.8 m/s^2); q is the natural inflow to the landslide barrier lake and t is time. Discharge is the mass balance considering the loss in volume of the barrier lake and upstream inflow. A is the water surface area, which is considered as a function of water level H. The erosion rate of the spillway $\frac{\Delta Z}{\Delta t}$ is calculated by considering the critical shear stress:

$$\frac{\Delta Z}{\Delta t} = \frac{k(\tau-\tau_c)}{a+b(k(\tau-\tau_c))} \quad (3)$$

$$\begin{cases} \tau = \frac{\gamma n^2 V^2}{R'^{1/3}} \approx \frac{\gamma n^2 V^2}{h^{1/3}} \\ \tau_c = \frac{\gamma n^2 V_c{}^2}{R'^{1/3}} \approx \frac{\gamma n^2 V_c{}^2}{h^{1/3}} \end{cases} \quad (4)$$

In this study, the erosion rate at the base was assumed equal to the lateral wall for simplicity; a and b are two coefficients, the recommended value of a is 1.1 for landslide dams; k is a coefficient which is usually equal to 100 based on field-scale measurements (Chen et al., 2014). The bottom shear stress τ, is calculated from the Manning formula, as in Equation (4), τ_c is critical shear stress, V is velocity of the flood. Here, γ is the specific weight of water (9.8 kN/m^3); n is the roughness coefficient; R' is the hydraulic radius, which is approximated by h due to the channel B_c being sufficiently wider than the average flow depth h.

Generally, most landslide dam breach studies choose values of "a = 1.1" and "b = 0.0007" (e.g., Tangjiashan landslide dam, (Chen et al., 2014). Both dam are made of loose soil in a state of low compaction. The very loose nature and relatively small particle size of Baige landslide dam materials mean that it is more erodible, therefore, we adopted a b value of 0.0003 in this study. We used a roughness n of 0.025 m$^{-1/3}$·s, based on a general value for similar river dynamics settings (Carling et al., 2010; George et al., 2017). Using Wang's (2008) formula for calculating the critical velocity

of a mixture of different size particles, the critical velocity of the landslide mixture $V_{d,c}$ was calculated as:

$$V_{d.c} = K\sqrt{2g\frac{\gamma_s - \gamma_w}{\gamma_w}d} \quad (5)$$

where d is the average particle diameter of the dam material; γ_s is the unit weight of dam material, in this study 2.56g/cm^3; K is a coefficient, in mixed sand it is in the range 0.89–0.93. From field investigation, a representative particle D_{90} of 0.24 m was identified and the related critical entrainment velocity was calculated as 2.41 m/s.

3.3 Controlling landslide dam morphologic parameters

Dam height is determined by the local elevation difference between the dam surface and local riverbed where flow passes through the dam. The critical dam surface elevation is that which determines the maximum elevation of the upstream lake, when the lake's elevation is higher than the critical elevation, the flow would start to overtop the dam. This value determines important outburst flood parameters such as lake volume, peak discharge, and in this study, we defined it as the effective dam height (H_e), which is calculated from DEM data (Fig. 4a). The effective dam height was obtained from cross-section data along the river, in which cases the maximum height of each section's minimal elevation was defined as the effective dam height, which determines the maximum lake volume before the dam breach.

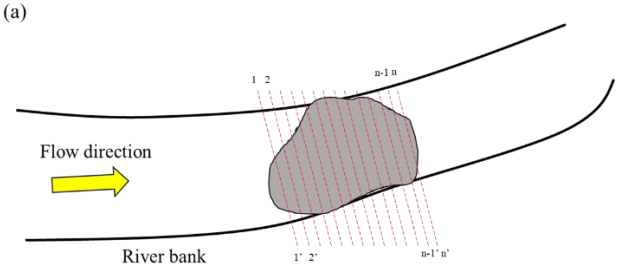

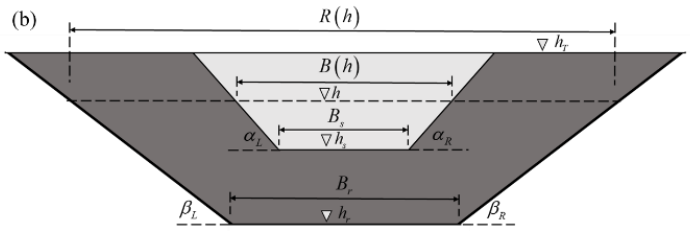

Fig. 4. Breach definition: (a) Plan view of landslide dam in river channel showing cross sections used for calculation of effective dam height; (b) Geometric relationships between dam, spillway and river relevant to determination of the Narrowing number *N*r.

To determine the degree to which a river section is occupied by landslide materials, we defined a new dimensionless number, the narrowing number N_{r}:

$$N_{\mathrm{r}}(H) = \frac{R(H)-B(H)}{R(H)} \quad (6)$$

where $N_{\mathrm{r}}(H)$ is the degree of narrowing at elevation *H;* $R(H)$ is the initial river width at elevation *H;* $B(H)$ is the breach width at elevation *H.* If the outburst flood erodes the initial river bank, $B(H)$ is smaller than *R(H)* so that $N_{\mathrm{r}}(H)$ stays below 1. If $N_{\mathrm{r}}(H) = 1$, the landslide occupies all the area in the elevation *h*; if $N_{\mathrm{r}}(H) = 0$, no landslide material occupies the elevation *H*. The parameter can be used to compare the breached spillway and initial river cross sections. No DEM data were available for one of our comparator events, the Xuelongnang landslide dam that occurred c. 1000 years ago; in this case, we assumed that river geometry upstream and downstream of the dam was similar to initial river geometry at the dam site for calculation of $N_{\mathrm{r}}(H)$.

4 Results

4.1 Dam geometric characteristics in the Baige events

DEMs show that the height of the landslide debris on the distal side is higher than the height

on the proximal side of both landslide dams (Fig. 5a). Surface elevations of the dams can be classified into two sub-areas: (1) red and yellow area, above 2970 m; (2) green and blue area, below 2970 m. The difference DEMs (Fig. 5c) show that most of the erosion in the second landslide took place in the second sub-area (SB-2), so would have had very little influence on the dam's geometry of the first sub-area (SB-1).

Cross sections (Fig. 5b) show that average elevation differs on either side of the dam; this is important as elevation controls where the dam breach is initiated. Usually, the dam cross section is assumed to be a regular trapezoid for breach calculations. However, in the current case, the breach was initiated in the lower, SB-2, therefore the dam cross section cannot be treated as a regular trapezoid. The value of H_e (defined in section 3.3) was calculated from the lower right part of the dam which is in SB-2.

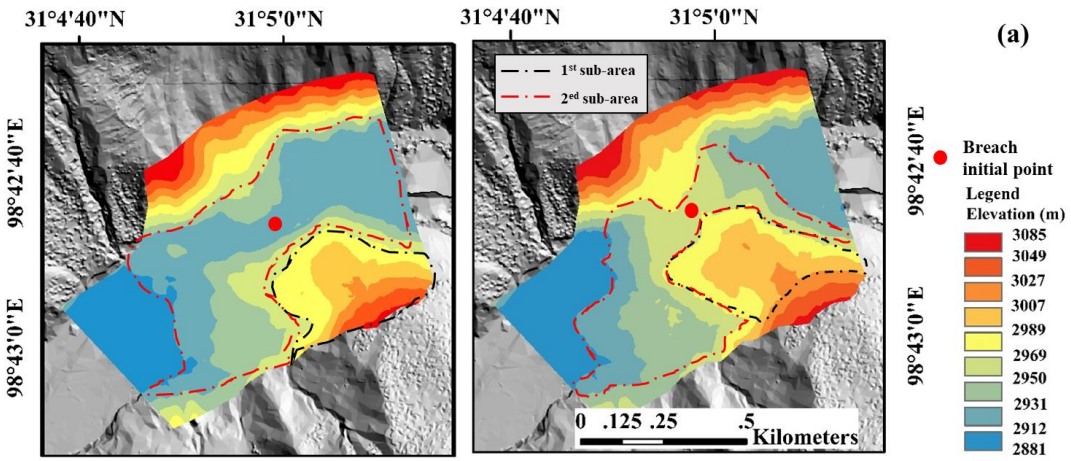

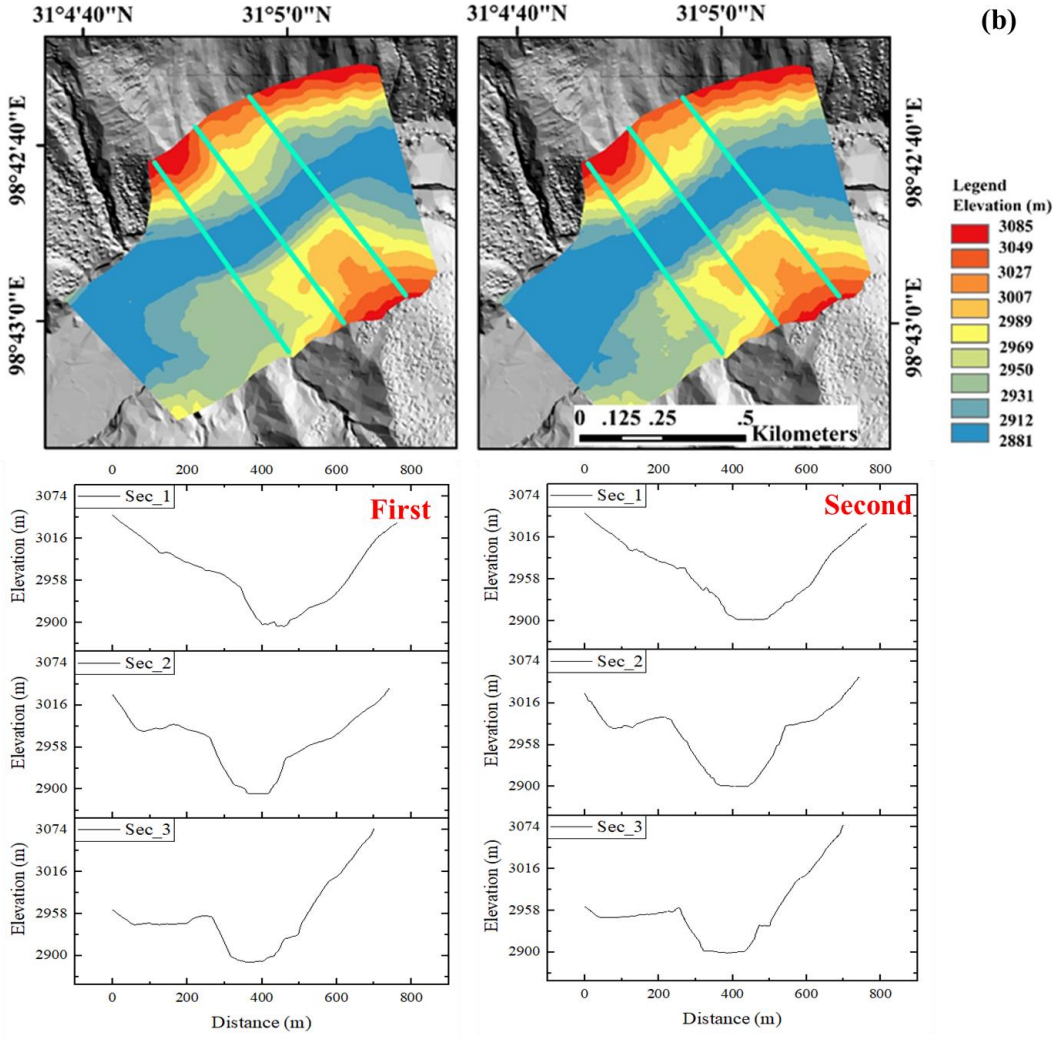

263

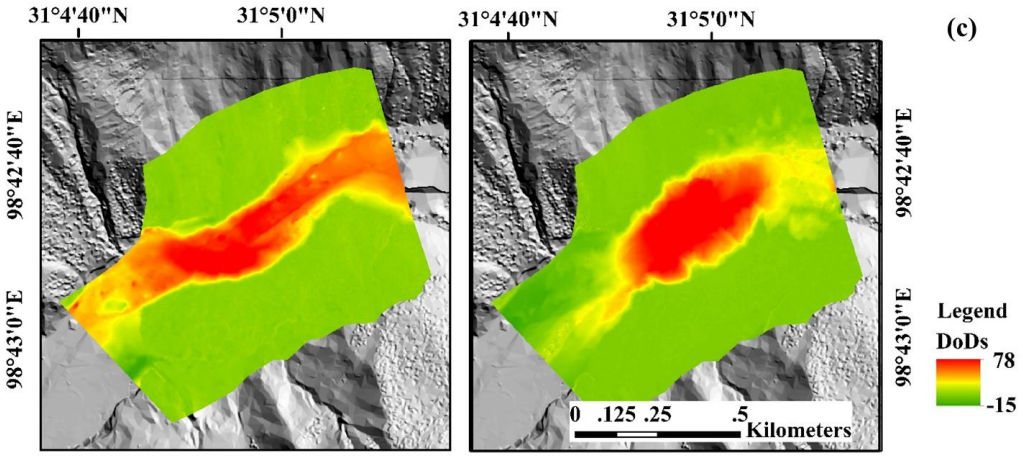

264

265 **Fig. 5.** (a) Elevation DEM of the first (left) and second (right) landslide dams at Baige, left is

266 downstream in both images; (b) Cross section location (top) and profiles (bottom) for the two

Baige event, section profile was viewed from upstream to downstream; (c) DoD showing elevation changes resulting from outburst floods. Most erosion was focused on the SB-2, with little elevation change in the SB-1 (see (a) for location of sub-areas).

We analyzed erosion processes in the two dam breaches using DEMs of difference (Fig. 5c). The initiation point for the first breach was located close to the center of the SB-2. After the first dam breach, a new channel with a steep channel slopes (around 40^{o}), which is similar to the angle of repose for soil) was eroded in the SB-2, but the geometry of the SB-1 was not altered. The initial breach location of the second outburst flood was at a higher elevation, but was also close to the center of the SB-2. Like the first event, the powerful outburst flood eroded a new, steep-sided, deep channel in the SB-2, but it had little impact on the SB-1 (Fig. 5 b). Cross sections of the two eroded channels are almost all trapezoidal with similar widths of channel bed and two steep sides (Fig. 5b).

After the first dam breach, 20.5×10^{6} m^{3} of sediment remained in the Jinsha river and the outburst flood transported 4×10^{6} m^{3} of sediment downstream, which represented only 16.3 % of the total volume of the first landslide dam. A trapezoidal spillway with a bottom width of 60 m and height of 60 m was formed after the first dam breach, with a vertical incision depth of 40.86 m which is 64.14 % of the H_e of the first dam. The spillway became the new river channel after the first dam breach. The width of spillway bottom in both cases is smaller than that of the original river.

4.2 Back analysis of second dam breach and prediction of natural dam breach for the second dam

The first dam breach was a natural one, but the second dam was artificially excavated prior to breaching. The excavation was useful to reduce peak flood magnitude and downstream outburst

flood risk, but for our analysis and comparison with the first event, we need to determine the characteristics of what would have been the natural breach. Numerical simulation is an effective method to obtain information on the natural dam breach.

Before numerical simulation, we needed to clarify the relationship between lake volume and elevation of the upstream landslide dam. Using DEM data with a 20 m resolution, the relationship between lake volume and the free water surface (in the landslide dam) elevation is shown in Fig. 6.

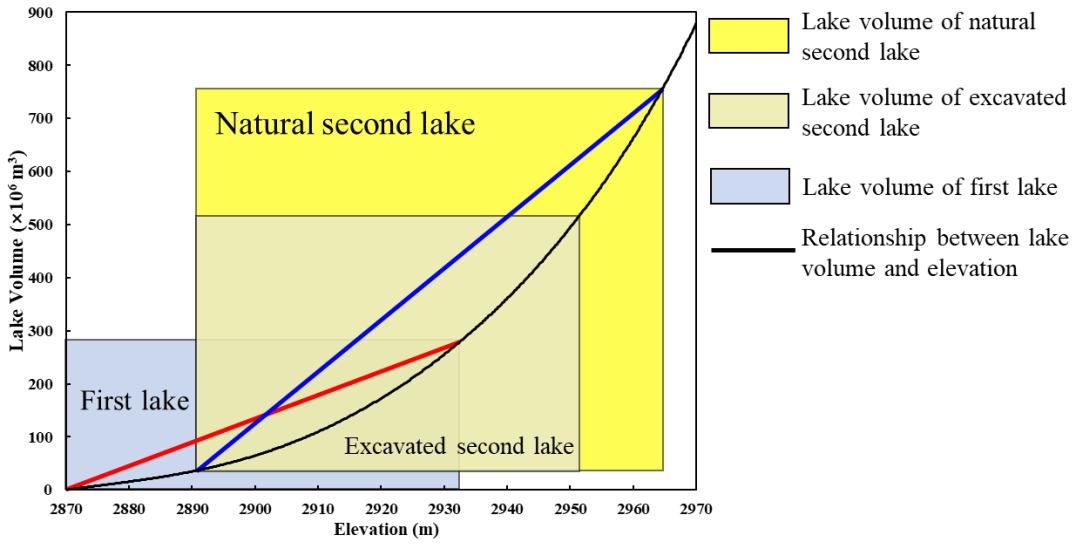

Fig. 6. Vertical lifting provided by the first dam increased blocking efficiency. The black curve is relationship between lake volume and elevation, changed. The slopes of red line and blue line are the rates of change of the volume per meter elevation change (see text for details).

The discharge curve for the simulated outburst flood from the artificial second dam breach at Baige generally fits well with the measured data (Fig. 7). However, at around 19.83 h on November 13, there is a small fluctuation in the measured discharge that is not reflected in the simulation; the short-lived decrease in discharge might have been caused by a large spillway side-wall collapse. Overall, the good match shows that the simulation results for the second dam breach are reliable.

Sensitivity analysis for the empirical coefficients of erosion were conducted, after Chen (2020), and included in the Appendix. The most sensitive parameter is '*b*', which could produce a change of 15% on peak discharge. The maximum time difference is 72 minutes.

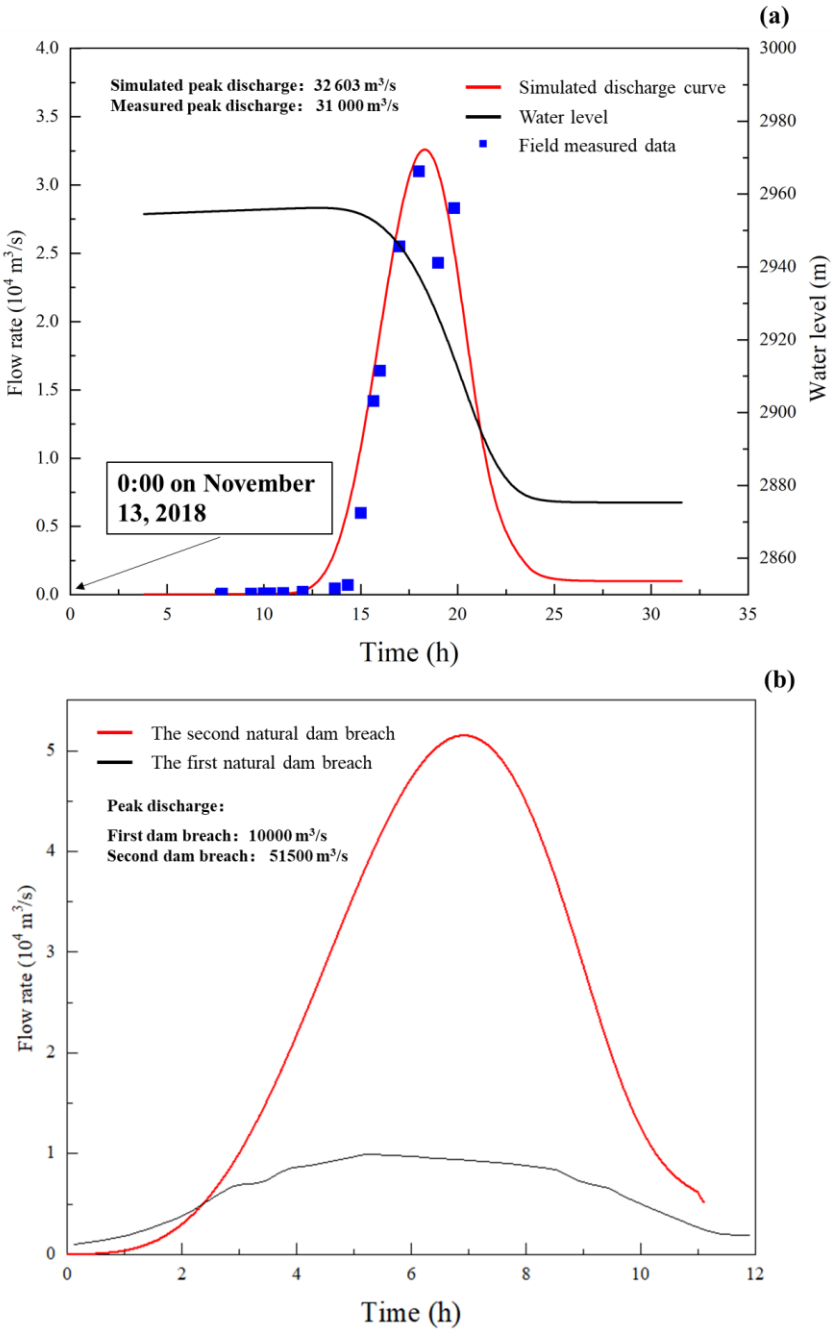

Fig. 7. Simulated hydrographs: (a) Simulated discharge curve for the artificial (after excavation) second dam breach; (b) Simulated natural discharge curve for the second dam breach

compared with the first dam breach.

For prediction of the natural dam breach, most of the input parameters remain the same as the simulated artificial/excavated dam breach, but with an elevation of 2966 m and initial channel width of 0 m. The resulting peak discharge for a natural dam break in the second event is 5.15×10^4 m^3/s, which is more than five times that of the first event and 1.66 times that of the artificial dam breach (Fig. 7b). Artificial excavation resulted in an H_e value of 13.48 m which is 16.34% of the initial H_e, while peak discharge decreases by 39.8 % compared with the no excavation condition. Clearly, artificial spillway excavation plays an important role in landslide dam risk mitigation.

4.3 Effective dam height dominates local peak discharge

The volume of the first landslide dam (2.45×10^7 m^3) was almost three times that of the second landslide dam (8.5×10^6 m^3). It is surprising therefore, that the second landslide generated a catastrophic outburst flood event with a much higher peak discharge compared with the first event. The volume of the second barrier lake (7.8×10^8 m^3) was more than twice that of the first barrier lake (2.9×10^8 m^3). To identify the key factors controlling the different responses, we compared a range of dimensionless parameters for the two natural events (Table 2). We normalized the H_e value, peak discharge, lake volume, potential energy, and dam volume parameters using the average width of the Jinsha river in Baige County B_r, which is 93 m, the upstream base flow rate of the Jinsha river Q_b which is around 1000 m^3/s (Wei et al., 2019) and the volume of the first landslide dam.

Table 2 Comparison of dimensionless parameters for the two natural dam breach cases

Dimensionless parameter	Formula	Physical meaning	1st landslide	2nd landslide	2nd/1st
$\bar{H}$	$\frac{H_e}{B_r}$	Geometry ratio of dam height and width	0.89	1.03	1.16

$\overline{Q}$	$\frac{Q_p}{Q_b}$	Ratio between maximum local flow rate of one blocking event and base flow	10	51.5	5.16
$\overline{LV}$	$\frac{LV_n}{V_1}$	Ratio of blocked lake volume and dam volume	11.84	35.51	3.0
$\overline{PE}$	$\overline{HLV}$	Representative upstream lake potential energy	10.54	36.58	3.47
$\overline{DV}$	$\frac{DV_n}{DV_1}$	Volume ratio between successive landslides and first landslide	1	0.35	0.35
$\overline{AV}$	$\frac{AV_n}{V_1}$	Ratio of accumulated dam volume to 1st dam volume	1	1.16	1.16

The parameters in Table 2 fall into two classes: (1) lake volume, peak discharge and potential energy, which all have quite high values; (2) dam height, dam volume and accumulated volume, which all have low values. Comparison of parameters for the second landslide with those for the first shows the greatest increases are in peak discharge, lake volume and potential energy. The ratios for accumulated dam volume and H_e are a little over 1, indicating little difference between the two events, but the dam volume ratio is below 1, indicating a decrease. These results are similar to those discussed by (Peng, 2012), in which lake volume and potential energy are strongly correlated with peak discharge. Overall, the comparison shows that H_e is a positive parameter that affects other parameters: it is axiomatic that dam volume has a fixed relationship with H_e, which determines lake volume and potential energy.

To investigate the relationship between H_e and peak discharge within the elevation range of the spillway we ran numerical simulations for different dam height scenarios. If the second landslide occurred very soon after the first natural dam breach, it would be easy to fill the lower SB-2 and form a new higher dam. Based on this assumption, we tested a dam elevation range of 2933.7 to 3011 m, where 2933.7 m is the elevation of the surface of the first dam in the SB-2 and 3011 m is the highest elevation of the first sub-area (Fig. 8a). Soil erodibility and geometry were set at the

same values as for the natural discharge simulation for the second event.

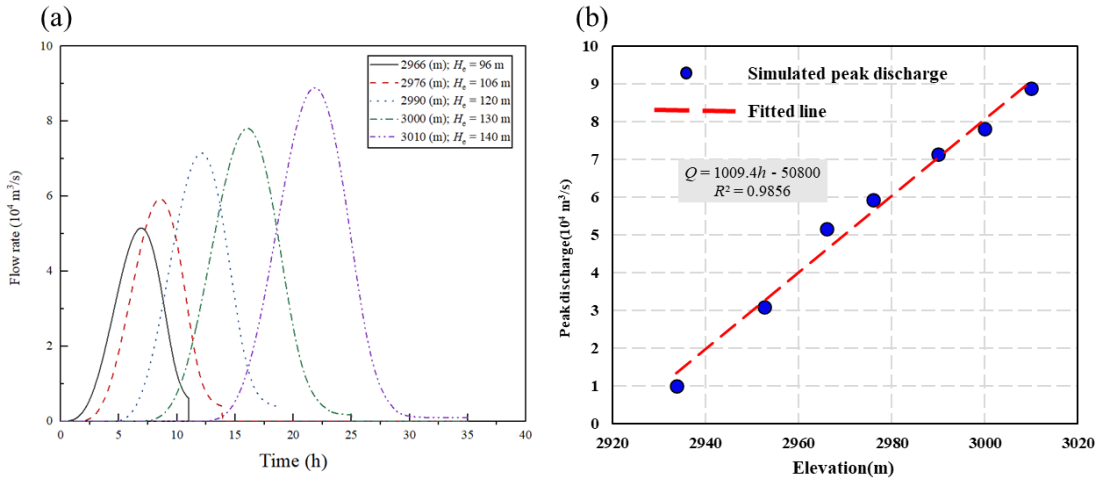

Fig. 8. Simulated discharge curve of different effective dam heights and relationship between related peak discharge and effective dam height at the Baige a) The graph shows discharge curve of dam breach for different dam elevation scenarios. b) linear relationships between peak discharge and effective dam height for different elevation scenarios.

If the second landslide dam had a greater volume, sufficient to fill the spillway of the first landslide dam, and breach initiation was at an elevation of 3000 m, peak discharge would be 7.92 $\times 10^4$ m^3/s (79.2 times base flow). If breach initiation occurred at 3011 m elevation, the peak discharge would be 8.84$\times 10^4$ m^3/s (88.4 times base flow). Overall, the results show a strong linear relationship between peak discharge and H_e for the range of spillway elevations tested, with R^2=98.6% (Fig. 8b). The results means that for every 1 m increase in H_e, peak discharge increases by 1009.4 m^3/s, which is equivalent to the base flow rate of the upstream Jinsha river. Evidently, H_e determines lake volume and potential energy (due to fixed upstream river geometry) at Baige, which determine peak discharge of landslide dam outburst events.

4.4 First landslide increases risk of second outburst flood by narrowing and lifting the riverbed

We investigated variations in the spillway cross section geometry in response to successive landslide and dam breaching using *N*r values. Four representative time periods were examined: (1) after the first landslide, before the first dam breach; (2) after the first dam breach, before the second landslide; (3) after the second landslide, before the second dam breach; (4) after the second dam breach. Cross sections within the central part of the dam (Fig. 9a) show similar features present on both landslide dams, with three elements: (1) higher left side in the SB-1; (2) lower side in the SB-2; (3) narrow central area with very steep sides. Figure 9b shows how N_r varies with elevation. Below the SB-2, a N_r of 1 shows that elevation in this range was totally blocked. *N*r shows great variation in the steep slope area. N_r is 0 above the higher SB-1, indicating no sediment blockage.

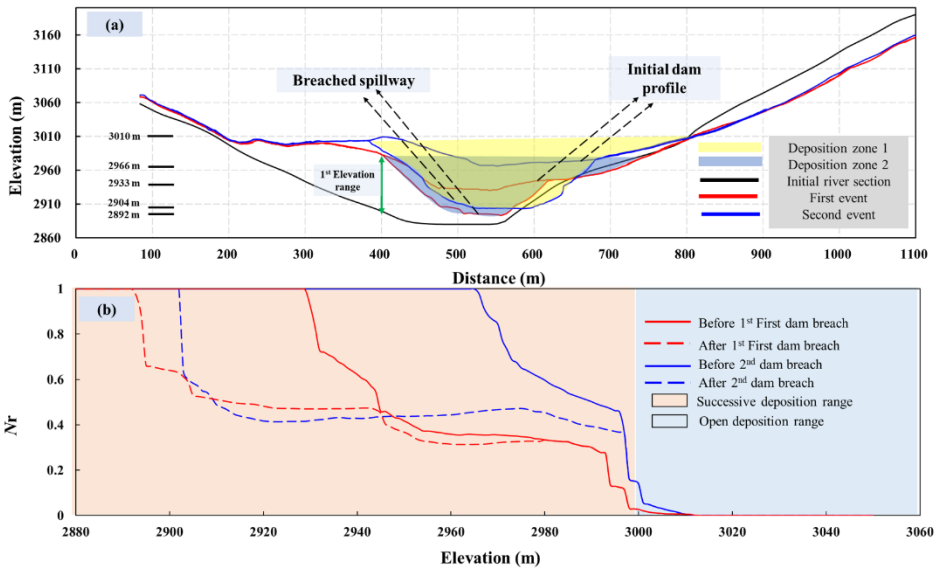

Fig. 9. Variations in cross section geometry around the center of the landslide dam. L1 and L2 are the elevation difference between river bottom and breach bottom of each case. *N*r is the

narrowing number at different elevations.

After the first landslide, the average elevation of the left side of the landslide dam was 3000 m and of the right side it was 2935 m, giving an elevation difference of 65 m which is very similar to the H_e of the first dam (63.7 m). *N*r is around 0.35 in the steep slope zone. A regular trapezoidal cross section was formed after the first dam breach, with a bottom width and height of about 60 m and side walls slopes of almost 40.6°. The first outburst flood did not reduce the *N*r of the SB-1, which is still close to 0.35, but the river was strongly narrowed, with the *N*r of the newly incised area of around 0.4–0.5. After deposition of the second landslide, the elevation difference between the two sides is 30 m, which is 31.25% of the H_e of the second dam (96 m). After the second dam breach, the *N*r value of the steep slope area decreased from 1 to 0.5. However, the landslide deposit had little influence in the SB-1. The outburst flood cuts a similar regular trapezoidal section to the first breach that has little influence on the *N*r value in the SB-1 and the *N*r value in the steep slope zone is around 0.5. Moreover, we analyzed *N*r value along dam (see Appendix A3).

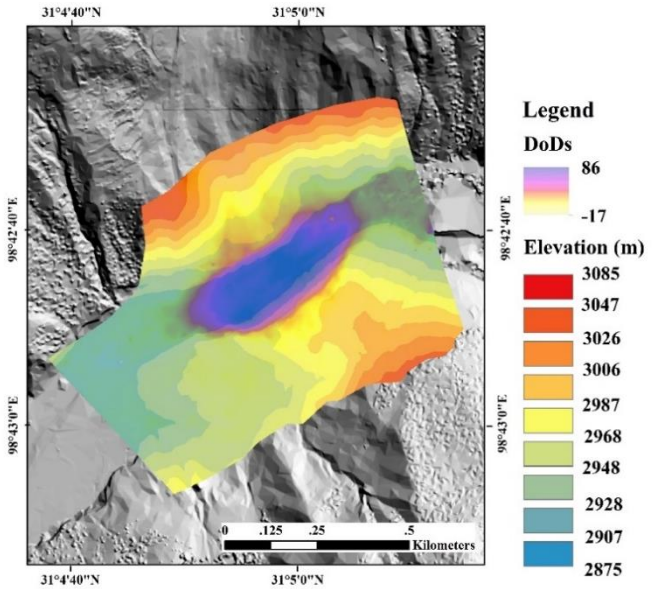

Fig. 10. DEM of the Baige landslide deposition zone showing DoD for the central area after

388 the second landslide. Debris from the second landslide filled the spillway of the first breach.

389 DEM analysis shows that the first landslide deposited material on the opposite river bank, in
390 the form of a runup deposit. The runup deposit provides a steeply sloping area that exhibits a huge
391 elevation range and encourages overtopping in the lower SB-2. In this range, *N*r is around 0.35. As
392 the outburst flood transported only a little debris in the SB-1, with most material in the SB-2, the
393 central part of the dam was still very narrow (*N*r = 0.5) in the elevation range of the newly formed
394 spillway and initial steep slope area. Furthermore, the initial valley side gradient of 26.6 degrees
395 allowed the first landslide to travel a long way, but the high (40.6°) gradient of the eroded spillway
396 banks would have significantly slowed the motion of the second event. The spillway formed by the
397 first breach provides a large, narrow and contained deposition zone (elevation difference between
398 spillway bottom and top is 103 m) for the second landslide. Accordingly, although the second
399 landslide was smaller in volume, almost all the material was deposited in the spillway, producing a
400 very thick mass (large elevation range) with a large H_e value (Fig. 10).

401 The two outburst floods eroded regular cross sections with width almost equal to depth, which
402 limits the potential for lateral erosion and decreases the *N*r. The formation of similar sections in the
403 two events could be due to the similar erosion characteristics of the outburst floods. Most models
404 assume a linear relationship between incision depth and lateral erosion (Fread, 1988; Chen et al.,
405 2014; Zhang et al., 2019; Zhong et al., 2020), or between vertical cutting rate and lateral erosion
406 rate (Osman and Thorne, 1988; Cantelli et al., 2007). The outburst flood cannot fill the whole
407 channel depth, so that the section of channel bank above the free surface collapses during lateral
408 basal erosion (Cao et al., 2011; Chen et al., 2014; Walder et al., 2015) and attains a slope around the

409 angle of repose for the bank materials.

410 Generally, the emplacement of a landslide dam raises the local elevation and forms a knickpoint.
411 Most outburst floods are not able to erode the dam completely to the initial river elevation due to
412 the limitation of upstream storage. The variation in elevation range for Nr = 1 reflects this local
413 elevation lifting. The first outburst flood did not remove all the dam sediment, leaving a spillway
414 with a bottom elevation 22.84 m higher than initial riverbed. The second dam lifted the riverbed to
415 33.81 m. Natural geometry determines the volume-elevation relationship; if a landslide dam is
416 emplaced at a higher elevation, the same increment of H_e would be able to impound more water,
417 which increases the blocking efficiency. On average, the ratio between maximum lake volume and
418 increase in H_e is 4.55×10^6 m^2 for the first dam (red line in Fig. 6) and 10.64×10^6 m^2 (blue line in
419 Fig. 6) for the second dam. The blocking efficiency of the second event was twice that of the first;
420 this process increases local outburst flood risk. The Yigong barrier lake, in the Yarlung Tsangpo
421 catchment in southeastern Tibet, has also been subject to repeated landslide blocking and lake
422 volume has increased significantly due to the effect of spatial superposition.

423 From empirical equations, the height of the dam formed by one landslide blocking event is
424 dominated by two factors: slope of the opposite valley side and valley topography (Wei et al., 2015;
425 Wu et al., 2020). Generally, the sides of the breach are steeper than those of a natural earth slope
426 (excluding rock slopes), and the breached dam has a narrower bottom width. Considering the initial
427 blocking condition, the variation in H_e after a determined landslide event contains two parts, which
428 can be calculated by:

$$H_{en} = H_N + H_B \tag{7}$$

$$\Delta H = H_{en} - H_R \quad (8)$$

where H_{en} is effective height of the new dam; H_N is dam height variation based on breached new geometry; H_B is bottom effective height of old breach; H_R is dam height where there is no old blocking condition; ΔH is the difference of dam height between blocking and no blocking condition. Qualitatively, if H_B is higher, a large impounded lake can develop upstream of the local dam and there is high potential for a catastrophic outburst flood such as occurred at Yigong barrier lake (Liu et al., 2019). Both the Yigong and Baige dams demonstrate clear characteristics of spatial superposition that has led to increased H_e values after successive events. Dam height and lake volume are two of the main parameters used to determine peak discharge in prediction models. For many elevation-lake volume models (no blocking condition), the slope of the relationship (volume increase per meter) is equivalent to a larger free surface area of the lake; the same change in H_e is related to much larger lake volumes at higher elevations. Successive landslides influence local morphology by increasing H_N and H_B for the next cases and produce high risk successive outburst floods despite a limited volume of landslide.

5 Discussion

5.1 Initial dam geometry influences the narrowing rate

The elevation range between the first and second sub-area, which was narrowed by landslide debris, provides a deposition zone for the next landslide and promotes formation of elevated H_e values. Furthermore, due to outburst flood erosion characteristics that tend to form a regular cross section, the spatial relationship between spillway and dam is relatively fixed. If a landslide forms a dam with a very large H_e value, and impounds a large volume of water upstream, the resulting

outburst flood has potential to transport almost all the deposition material without a narrowing effect. However, many cases have smaller lakes which might lead to a very high *N*r value in the river.

Due to the regular cross section of the spillway, the location of the breach initiation point influences the spatial relationship between spillway and dam. Four types of dam geometry can be considered (Fig. 11). If the kinetic energy of the landslide is high, it forms a dam that is lower on the proximal side and the breach initiation point is close to the proximal riverbank. The outburst flood erodes the proximal riverbank, but the higher distal side is intact (Fig. 11a). If the kinetic energy of the landslide is moderate, the breach initiation point tends to be in the middle of the lower proximal side. The middle lower part of the dam erodes and the proximal riverbank deposits and the higher distal deposits remain intact (Fig. 11b). Tangjiashan (Liu et al., 2010) blocking events follow this model. If the landslide has relatively low kinetic energy, the breach initiation point is close to the distal side; this mean that lower distal part is eroded (Fig. 11c), as a breach channel develops, with limited effects on narrowing. The Baige landslide dam belongs to this type. If breach initiation is close to the higher distal side, most material on the higher side is eroded (Fig. 11d), which would deduce narrow effects. Tanggudong dam belongs to this type (Song, 2015).

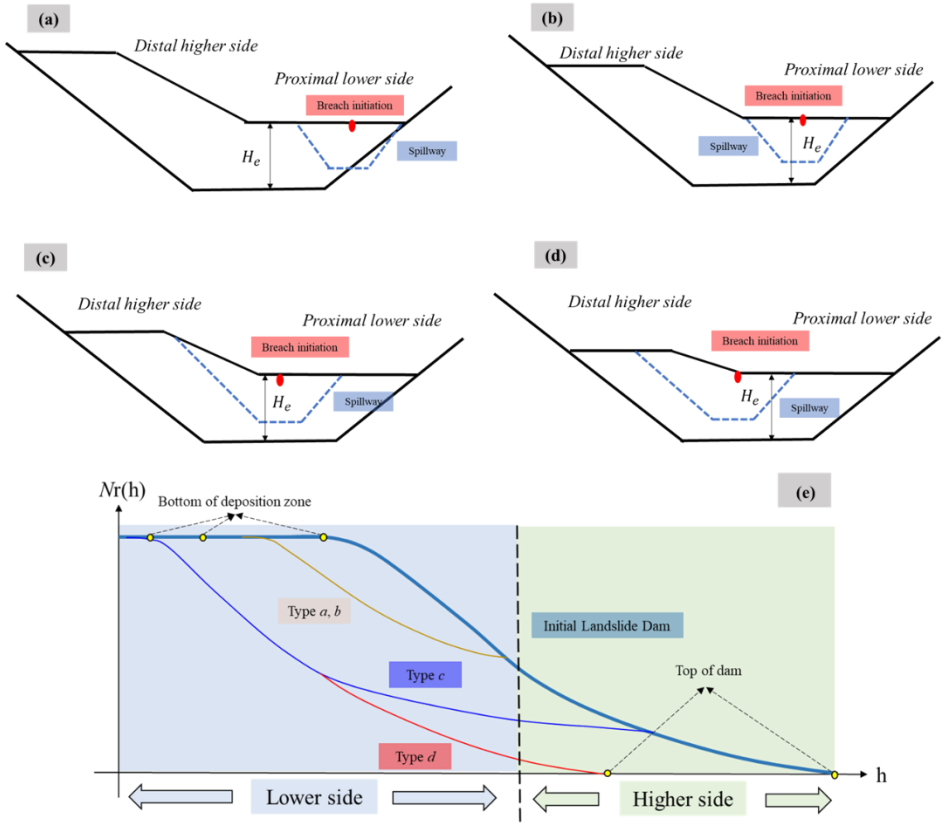

464

465 **Fig. 11.** Relationships between dam and spillway geometry. Red points indicate where the

466 dam breach initiated. The three yellow points in e are bottom elevation of breached dams. (a), (b),

467 (c) and (e) are the type a, b, c and d of dam and spillway geometries; (e) is the ideal narrowing rate

468 curve of the four types.

469 We calculated *Nr(h)* for the four dam geometries (Fig. 11e). With types *a* and *b*, the outburst

470 flood only affects the lower proximal side, a narrow river is maintained at a high elevation. With

471 type *c*, the outburst flood erodes and transports some debris from the higher distal side, it reduces

472 the risk of further erosion of the higher distal side. With type *d*, the outburst flood erodes significant

473 sediment from the higher distal side, the *Nr* value of high elevation range reduces and the risk from

474 initial dam blocking in this elevation range is significantly reduced.

5.2 Breached landslide dams increase local blocking and flooding possibility

Landslide dams or breached dam may persist for hundreds of years and block transport of sediment from upstream by lifting the local elevation (Korup and Tweed, 2007), the effects of this control on river morphology may persist for thousands of years (Wei et al., 2015; Liu et al., 2019). The concentration of narrowing in a fixed elevation range promotes the formation of new local blocking cases. To further investigate the narrowing effects on dam formation, we used a number of empirical models (see Appendix A2) to calculate critical conditions of river blocking for some previously published major landslide dams in southwest China. The calculated *N*r values of the dams lie in the range 0.3-0.7, yielding increased blocking factors in the range 1.13-3.33 (Fig.12), suggesting the initial dam significantly increased the potential for subsequent dam formation. The slope of the relationship between *N*r and the increase ratio ranges from 4.6 to 0.9 due to different calculation models employed (Table A2).

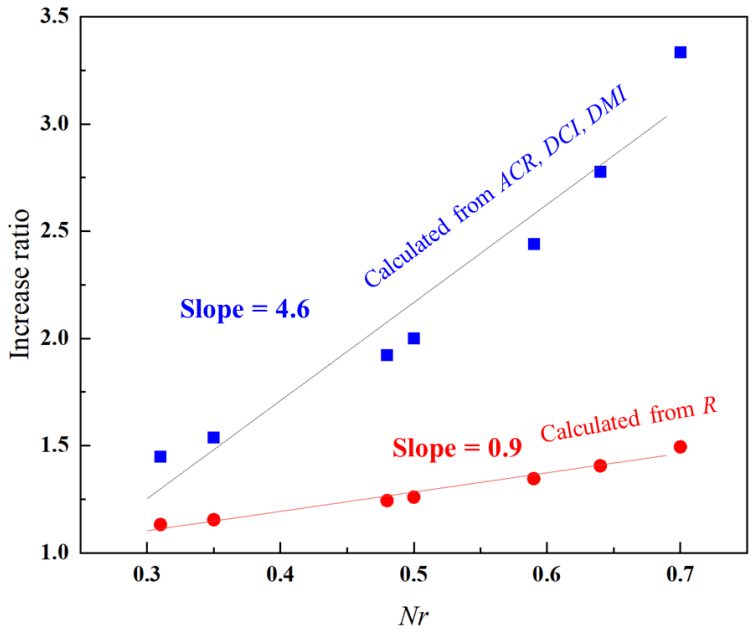

Fig. 12. Relationship between the *N*r values and the increase ratio and from field dams, blue points

are calculated from *ACR*, *DCI* and *DMI* models, red points are calculated from *R* model (see Table.A3).

Once a dam is emplaced, there is increased likelihood for a smaller volume landslide or lower energy landslide, to block the river than if there was no prior blocking. The relationship between *N*r and the increased ratio of likely blocking for different dams is proportional, indicating that more intensive initial narrowing is related to easier subsequent blocking.

5.3 Effects of inflow on evolution of dam geometry

Although a dam could stay in a river for many years, its geometry likely will change before the next landslide occurs, Factors that drive morphological change of the breached dam include earthquakes, rainfall, inflow and compaction, which might change H_N and H_B. The effects of inflow, including base flow and seasonal and outburst floods are discussed below.

Xuelongnang landslide dam (99°03′07.81″E, 29°29′10.85″N, which occurred more than 1000 years ago) is located in the upper Jinsha river, 213 km downstream of the Baige landslide dam. It is a rock dam with a D_{90} of about 1.2 m, so is unlikely to be eroded by base flow. A series of Google Earth images (Fig. 13) show changes to the dam spillway before and after the Baige outburst floods in 2018. In January 27, 2010 and March 8, 2015, several rocks are visible in the middle of the spillway (marked by the yellow box in Figs. 13a and 13b). The stable position in the six years between the two images indicates a lack of vertical erosion under prevailing seasonal flooding and base flow conditions. In the second 2018 Baige outburst flood, which had a magnitude equivalent to the 10000 year seasonal flood at Xuelongnang dam, the rocks were transported and formed a new aggregation downstream (marked by yellow box in Figs.13c and 13d, and plan view in Fig. 13f). A

new road was constructed at Xuelongnang from 2010–2015, to link the upstream lake area with the top of the landslide dam; the road foundations were built in landslide dam material, which was stable during the period (red box in Fig. 13 (a), (b)). After the Baige outburst flood, intensive erosion destroyed the foundations and part of the road (red box in Figs. 13c and 13d; aerial view in Fig. 13e). Over the nearly 10 year period of observation the spillway was not noticeably altered under base flow and seasonal flooding, suggesting these discharges are insufficient to transport spillway sediment in Jinsha river. The case study shows that dam geometry is persistent and landslide dams may be maintained in rivers for long periods of time, continuing to influence local outburst flood risk.

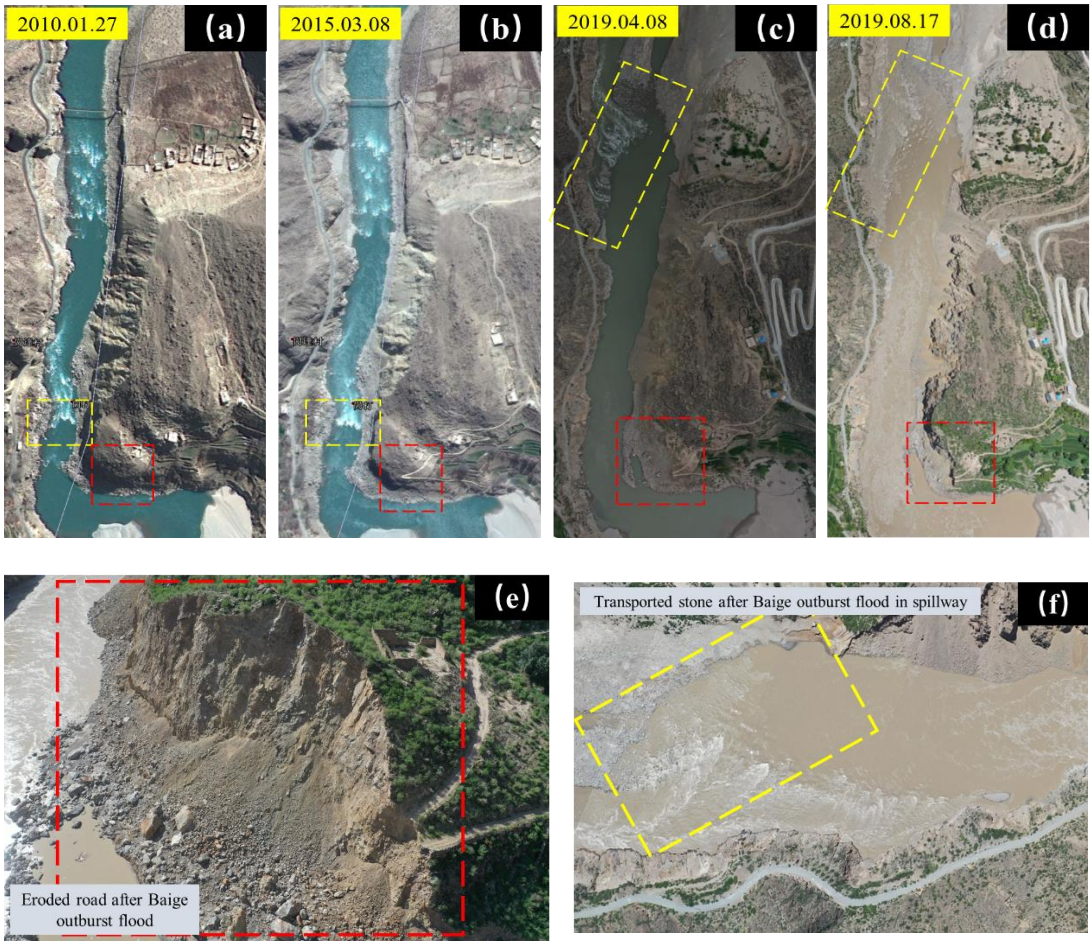

Fig. 13. Aerial images of the relict Xuelongnang landslide dam, Sichuan province, China. (a) Google Earth image taken on 01.27.2010; (b) Google Earth image taken on 03.08.2015; (c) Drone image taken 04.08.2019; (d) Drone image taken 08.17.2019, after the 2019 seasonal flood; (e) Eroded road after the second Baige outburst flood; (f) Aggregation of rocks downstream of Xuelongnang, after the second Baige outburst flood. Dashed yellow boxes mark location of large rocky debris and red boxes the location of a new road built from 2010–2015.

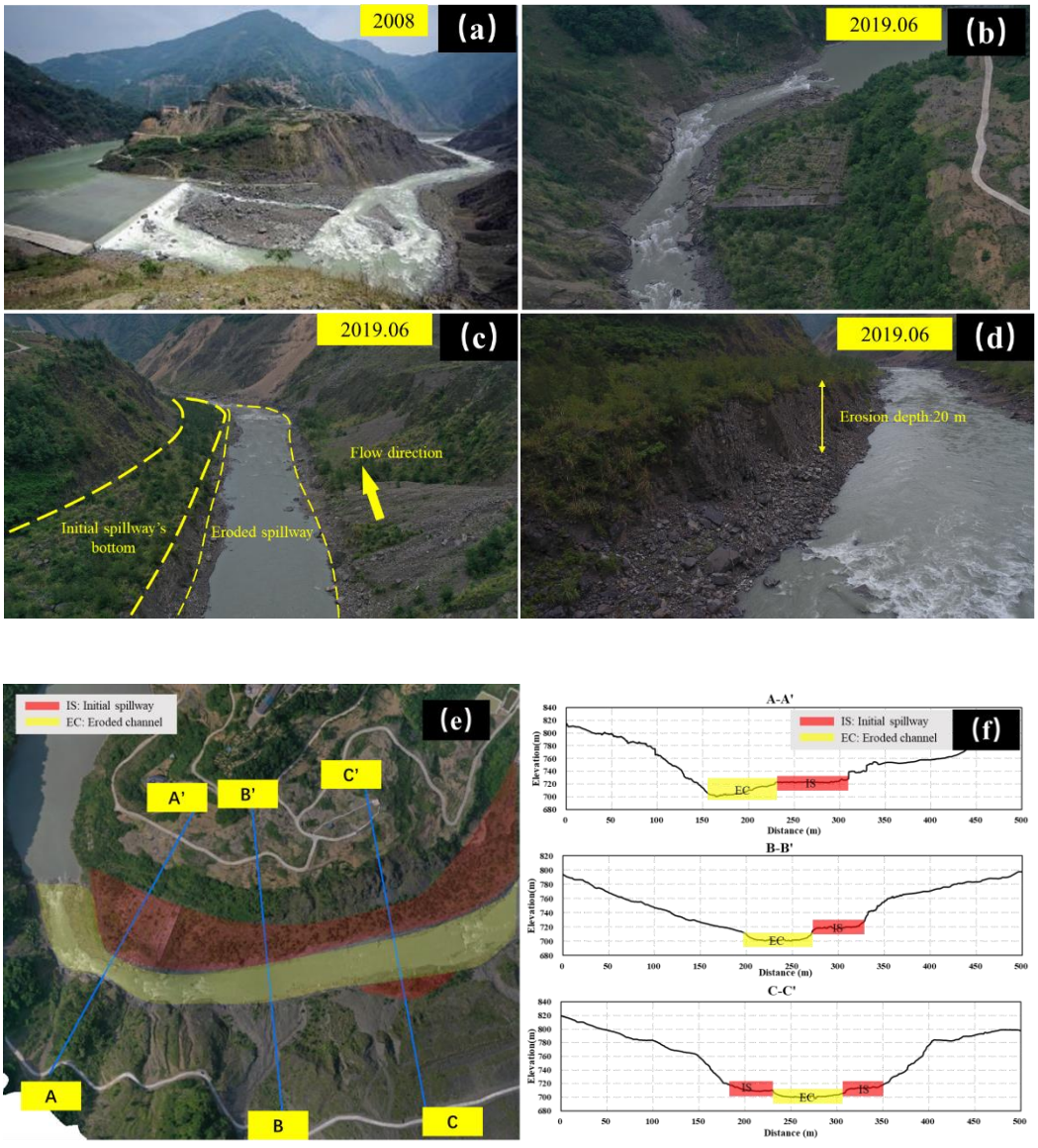

Fig. 14. Tangjiashan landslide dam, northern Sichuan, China. (a) Image taken after emplacement of the dam in 2008 showing concrete layer constructed to reduce incision; (b) Part of the concrete layer had been eroded by June 2019; (c) New spillway had been formed by June 2019; (d) Erosion depth of new spillway, June 2019; (e) Blue lines mark location of cross sections; (f) Cross sections showing profile of eroded spillway.

The Tangjiashan landslide dam was the largest failure caused by the Wenchuan earthquake in Beichuan County, northern Sichuan, in 2008. After dam breaching, a concrete block layer was constructed in the upstream part of the spillway to prevent vertical erosion (Fig.14a). Eleven years later in June 2019, due to erosion from base flow and seasonal flooding, some of the concrete blocks had been eroded (Fig. 14b). The spillway eroded laterally, forming a new channel to the right and leaving a platform on the left (Fig. 14c). Three cross sections derived from drone data (Figs. 14e and 14f) show the depth of erosion accomplished by 11 years of baseflow and seasonal flooding; around 20 m at sections A-A' and B-B' and 10 m at section C-C'. The Tangjiashan landslide dam is comprised of materials with a smaller particle size than Xuelongnang landslide dam, so the morphology of the spillway is continually evolving. Figure 14f shows that spillway erosion is unbalanced; this may be due to the intensive cutting ability of the outburst flood, as seasonal flooding and base flow are generally not of sufficient magnitude to drive erosion of the spillway bottom. Vertical erosion of the spillway formed a new narrower channel, inset within the original spillway margins.

544 **Fig. 15.** Drone imagery of Baige landslide dam, five months after the second dam breach. (a)
545 Erosion depth in spillway; (b) Overview of spillway showing active vertical incision and lack of
546 lateral bank erosion.

547 The material comprising the Baige landslide dam is very erodible and has been actively
548 modified by base flow since the second dam breach. Drone data from April 2019 shows vertical
549 cutting of 4.13 m in the upstream part of the spillway, achieved by base flow (Fig. 15). Like
550 Tangjiashan landslide dam, Baige's original spillway geometry includes no erosion on the left
551 spillway bank which belongs to the SB-1, so that the narrow part of the dam was not eroded.

552 Comparison of the three cases shows that the balance between dam composition and flow
553 dynamics plays a key role in dam evolution, stability and longevity (Fan et al., 2019a). Flow in a
554 spillway has different physical properties than normal river flow. Inflow approaches the initial
555 breach as weir flow which accelerates due to water head difference. Given the short length of the
556 spillway, it is difficult for the inflow thalweg to meander and erode laterally. Seasonal flooding and
557 base flow are sufficient to cut a smaller new channel in the spillway. If lateral flow erodes dam
558 material, collapse of the steep slope during vertical cutting could produce a large amount of debris
559 that could push the river away, thus protecting the spillway bank. Over a long period of time, vertical

cutting and infilling might lead to a continuous river longitudinal profile, but the two huge banks formed by the dam would still maintain the narrow river. Hence, the high risk posed by the narrowing effects of landslide dams persist until the dam is totally eroded.

6 Conclusion

Successive landslides in 2018 blocked the Jinsha river at Baige twice, with two outburst floods generated after overtopping of the dam. The volume of the first landslide was 24.5×10^6 m^3, with an H_e of 63.7 m, which generated an outburst flood with a peak discharge of 1×10^4 m^3/s. The second landslide, with a volume of 8.53×10^6 m^3, infilled and covered the first spillway to form a dam with an H_e of 96 m. After excavation, the elevation of the spillway base reduced by 13.48 m to 2952.52 m, forming an outburst flood with a peak discharge of 3.1×10^4 m^3.

Both Baige landslide dams comprised two sub-areas, the first a high elevation area (SB-1) to the left and the second a low elevation area (SB-2) to the right, with a steep slope between them. The first outburst flood cut through the dam and formed a huge depositional zone so that most materials of the second landslide were deposited in SB-2. Due to the irregular morphology of the dam, the first and second dam breach both initiated in the SB-2. The two outburst floods only eroded the SB-2 – the geometry of the Sb-1 was unchanged – forming a regular trapezoid spillway section with steep sides of around 40 degrees.

We adopted a numerical approach to predict the discharge curve of the dam breaches. The simulated peak discharge for the second outburst event was 3.26×10^4 m^3/s, which is close to field measurement. We used physical data from the excavated event to predict the peak discharge of a natural dam breach of the second dam, giving a value of 5.15×10^4 m^3/s. Based on a series of

simulation studies, the dominant parameter controlling peak discharge is H_e which determines local upstream potential energy and volume of the barrier lake. The parametric study shows there is a linear relationship between peak discharge and dam height elevation. The slope of the relationship is 1009.4 $m^3/s/m$, which means for every 1 m increase in dam height, peak discharge increases by 1009.4 m^3/s, which is equivalent to the average upstream base flow of the Jinsha river. After two floods, H_e values are 22.84 m and 33.41 m respectively.

Due to effective dam height dominating dam breaching (other than averaged dam height), a dimensionless number N_r was proposed as an indicator of the lifting and narrowing effect on the channel due to the landslide at different elevations. The difference in the elevation range of $N_r = 1$ between blocking events and the initial river level determines the H_e. The first landslide formed as a runup deposit due to its high momentum and covered a huge area of the SB-2 with N_r of around 0.35, occupying a high elevation range. Furthermore, as both outburst floods can only cut spillways with regular trapezoidal sections with N_r of around 0.5, the breached dam is still strongly narrowed. The area occupied a huge elevation range which related to range of local narrowing effects by first event.

The second-high risk outburst flood was affected by river bottom lifting and high elevation narrowing caused by the first landslide. Successive landslides could form successive high-risk outburst floods by spatial superposition. H_e represents spatial superposition. Run-up deposition, limited erosion ability of the flood and steep spillway banks provided a brake on the motion of the second landslide and account to the high effective height of the second dam.

A dam's geometry could influence subsequent landslide and dam breach behaviour. In terms

of managing flood risk, great attention should be paid to high elevation dams that narrow and lift the local river section. Excavation of a relief channel through the landslide deposits is an effective method to decrease the outburst flood risk.

Acknowledgments

This study was funded by the National Natural Science Foundation of China (41941019, 42077238) and the Research Fund Program of the State Key Laboratory of Hydroscience and Engineering (2020-KY-04). The authors would like to thank the National Natural Science Foundation of China (grant 41771045) and the CAS "Light of West China" Program.

Appendix

A1 Parametric analysis to soil erosion model

The key parameters of the erosion model are a, b and k. The parametric studies were conducted following (Chen et al., 2020). Each input parameter was varied by ± 10% and ± 20% separately whilst other parameters were kept constant. From these comparisons, the peak discharge has different sensitivity to these parameters. The most sensitive parameter is b, which related change rate of 15.65 % and 11.61 %. Parameter 'a' relate to 5.37 % to -5.0 %. 'K' relates to - 6.19% to 4.44 % (Table A1, Fig.A1., Fig.A2., Fig.A3.). The maximum time difference is 72 minutes.

Table A1 The change in peak discharge as parameter '*a*', '*b*' and '*k*' are varied.

Change rate	-20%	-10%	0	10%	20%
Peak discharge (change *a*)	34355	33456	32603	31765	30970
Change in peak discharge	5.37%	2.62%	0.00%	-2.57%	-5.01%
Peak discharge (change *b*)	37705	34939	32603	30574	28818
Change in peak discharge	15.65%	7.17%	0.00%	-6.22%	-11.61%
Peak discharge (change *K*)	30584	31675	32603	33376	34051

Change in peak discharge	-6.19%	-2.85%	0.00%	2.37%	4.44%

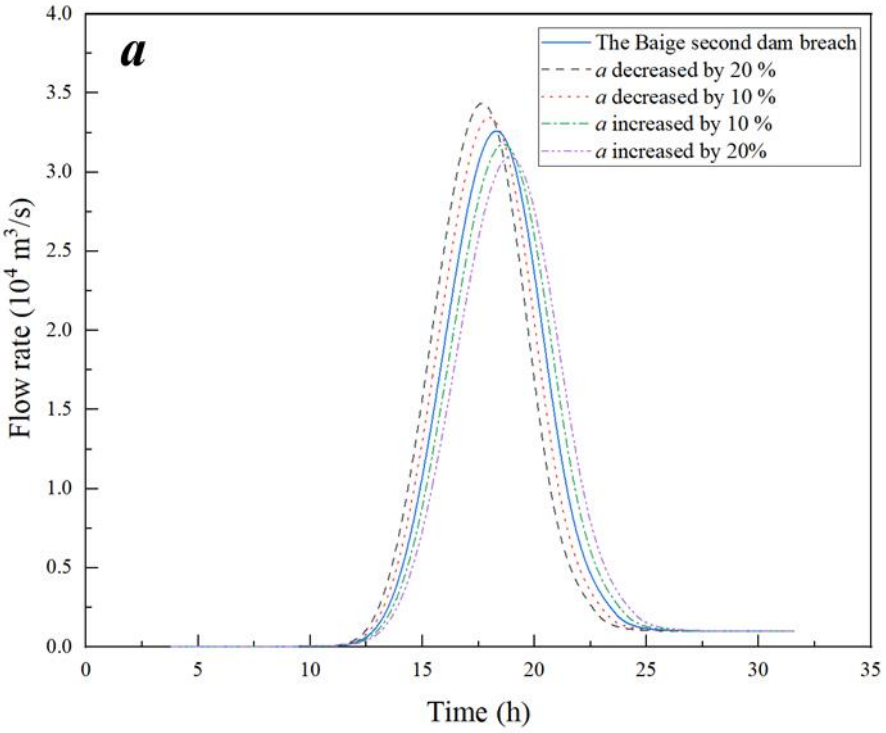

620

621 **Fig.A1.** Comparison of coefficient *a*

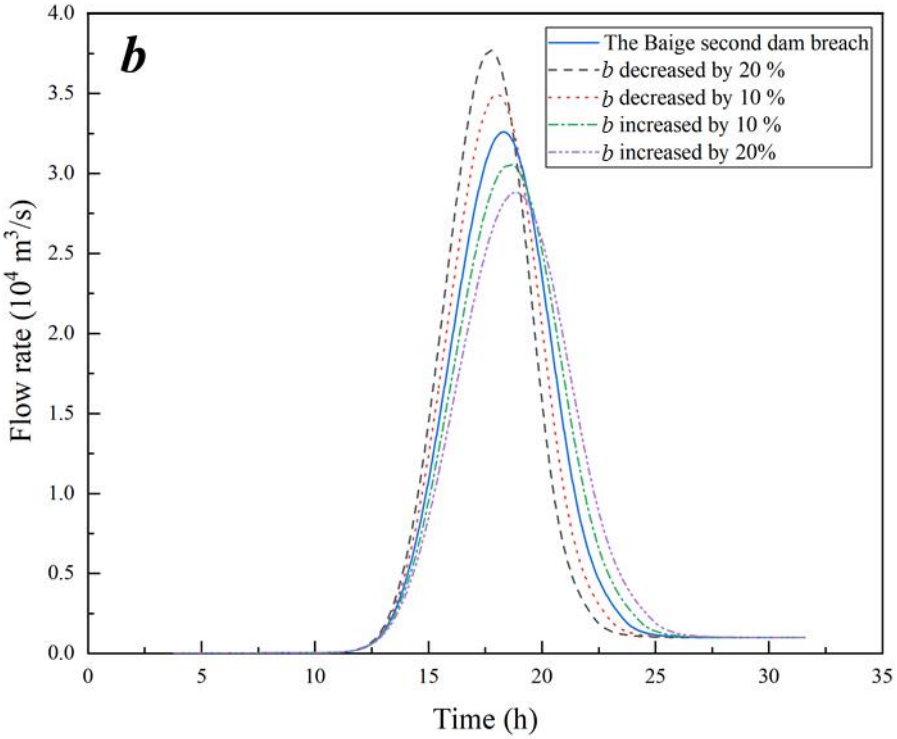

622

623 **Fig.A2.** Comparison of coefficient *b*

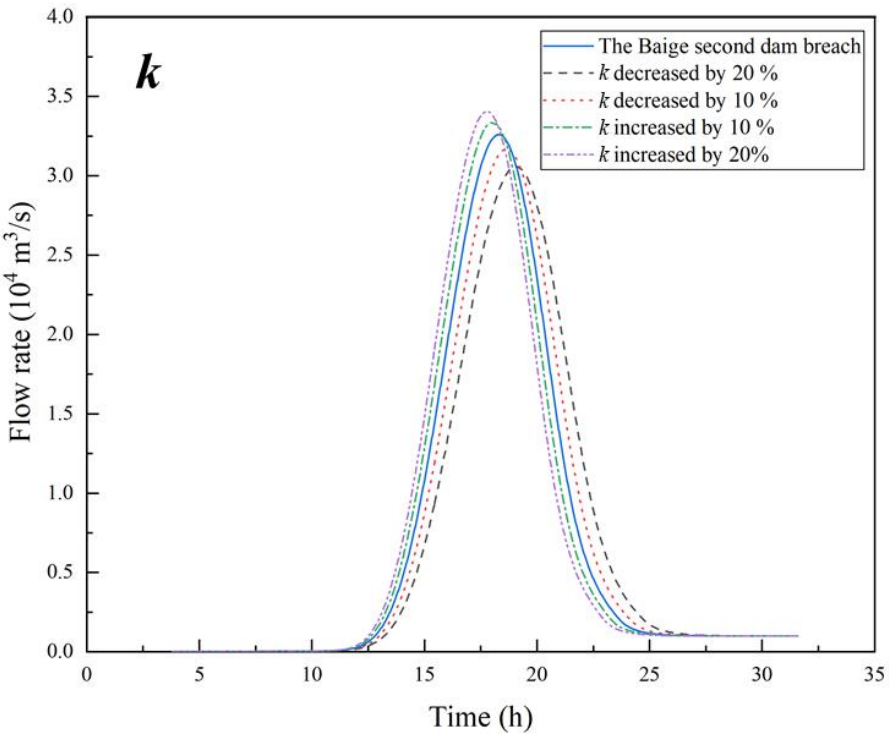

Fig.A3. Comparison of coefficient *k*

A2 Basic data for some field cases

The data for Figure. 12 are based on many breached dams (Table A3), the narrow rate was analyzed from DEM data. All the adopted calculation models are shown below:

Table A2 Models for estimating critical conditions of landslide dams

River blocking model	Critical value	Reference
$ACR = \frac{\bar{V}}{B_r}$	$ACR > 100$	Swanson et al., 1985
$R = \left(\frac{Q}{(45 \times 10^{-1.8tan\theta})g^{0.5}}\right)^{2/3} {B_r}^{1/3} L_B V_L^{-1}$	$R > 1$	Modified from Chen, 2015
$DCI = \frac{\bar{V} B_L h_L D_{30}}{Q_{P_5} B_r}$	$DCI > 0.002$	Ermini and Casagli, 2003
$DMI = \frac{2\rho_s \bar{V}^2 V_L}{\rho_w g h_r^2 B_r B_L}$	$DMI > 1$	Del Sasso et al., 2014

where *ACR*, *R*, *DCI*, and *DMI* are increase ratios; $\bar{V}$ is average velocity of the landslide; B_r is river width; q_w is upstream inflow rate per unit width; θ is river slope; g is gravity acceleration; V_L is landslide volume; L_B is dam length along river; B_L is landslide width;, h_L is landslide depth; D_{30} is the 30th percentile of the landslide particle size distribution curve; Q_{P_5} is 5 year return

period discharge; ρ_s is landslide density; ρ_w is water density; h_r is river flow depth.

Increase ratio is calculated by each model in Table.A2, by comparison between breached geometry and non-breached geometry. The subscript '*A*' of each model in Table.A3 means blocking possibility calculated from initial geometry, the subscript '*B*' means blocking possibility calculated from breached geometry. All the cases and information are shown in Table A3.

Table A3 Increased ratio of river blocking possibility associated with selected landslide dams in southeastern China (see Table A2 for definition of parameters), all the data are from Alos satellite, the resolution of DEM data is 12.5m.

Dam name	Date of blocking event	Average *N*r	Increase Ratio			
			$\frac{ACR_A}{ACR_B}$	$\frac{R_A}{R_B}$	$\frac{DCI_A}{DCI_B}$	$\frac{DMI_A}{DMI_B}$
Baige	2018	0.50	2.00	1.26	2.00	2.00
Tangjiashan	2008	0.35	1.54	1.15	1.54	1.54
Yigong	2000	0.64	2.78	1.41	2.78	2.78
Tanggudong	1967	0.31	1.45	1.13	1.45	1.45
Mogangling	1786	0.59	2.44	1.35	2.44	2.44
Xuelongnang	> 1000 years BP	0.70	3.33	1.49	3.33	3.33
Suwalong	> 1000 years BP	0.48	1.92	1.24	1.92	1.92

641 **A3 *N*r analysis along dam**

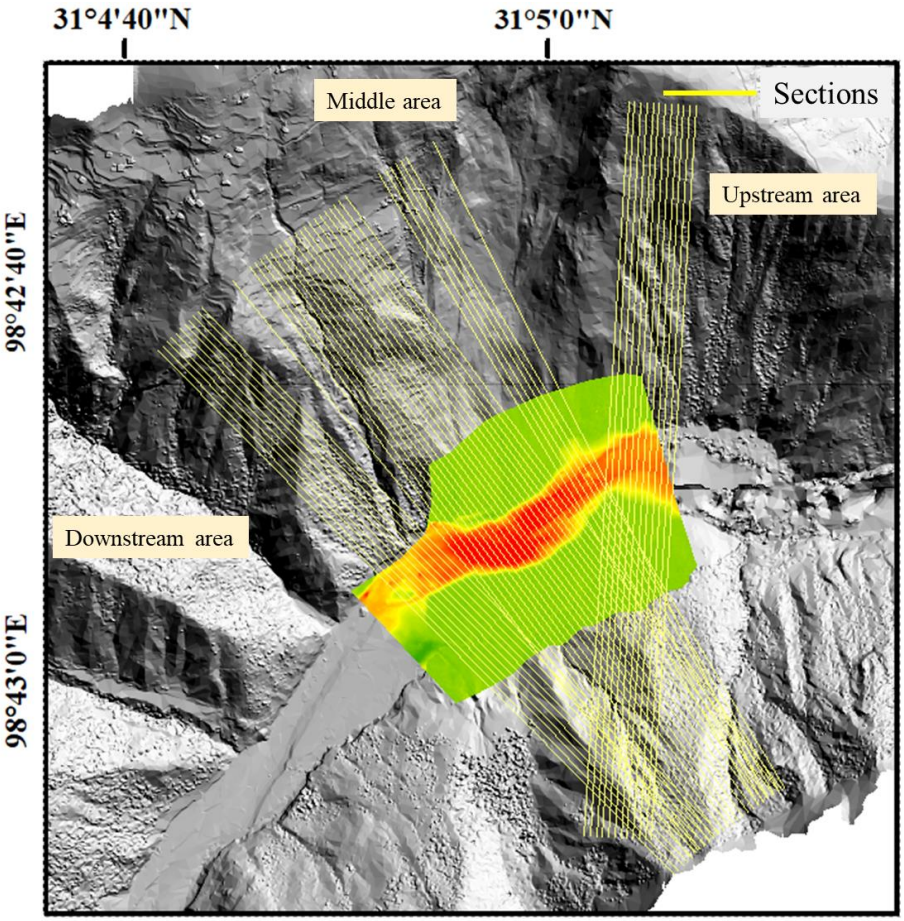

642

643 **Fig.A4.** Examples of the analysis of 51 sections. Flow direction is from right to left so
644 that three different areas were named as upstream area, middle area and downstream
645 area.

646 We analysis *N*r distributions from upstream to downstream, and divided them into four cases:
647 before and after the first and second dam breaches. During the analysis, 51 sections were extracted
648 from upstream to downstream (Fig.A4.). The distance between two sections is fixed at 20 meters.
649 We classify the dam into three parts: upstream area, middle area, and downstream area, as shown in
650 Figure A4.

651 The results showed that the upstream and downstream areas of the first landslide dam have a
652 higher elevation channel base than the second dam (Fig.A5. (a, c)). Consequently, the second dam

has less impact because the lowest elevation of the first landslide debris in the upstream area and downstream area is higher than the second landslide debris. However, the height cannot determine the barrier lake volume as it is too low, which means the local narrowing effects is limited. Nonetheless, the values of *N*r in upstream (*N*r = 0.1 ~ 0.2) and downstream (*N*r = 0.2 ~ 0.3) are lower than in the middle area (*N*r = 0.4 ~ 0.6), which means that the middle area has stronger narrow effects (Fig.A5 (b)). The effective dam height formed in the middle area, which determines the barrier lake volume. Therefore, the high narrowing affect can lead to a catastrophic flood triggered by a small volume landslide. Furthermore, landslide into this area (topography influenced) could easily form a higher dam.

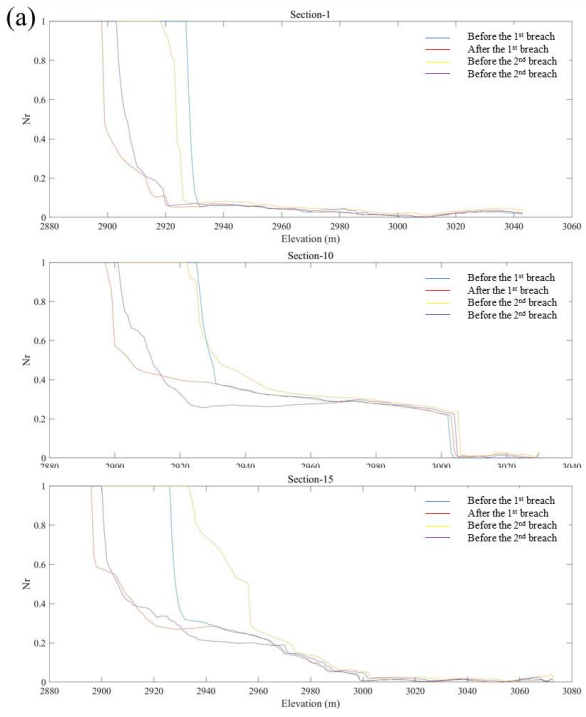

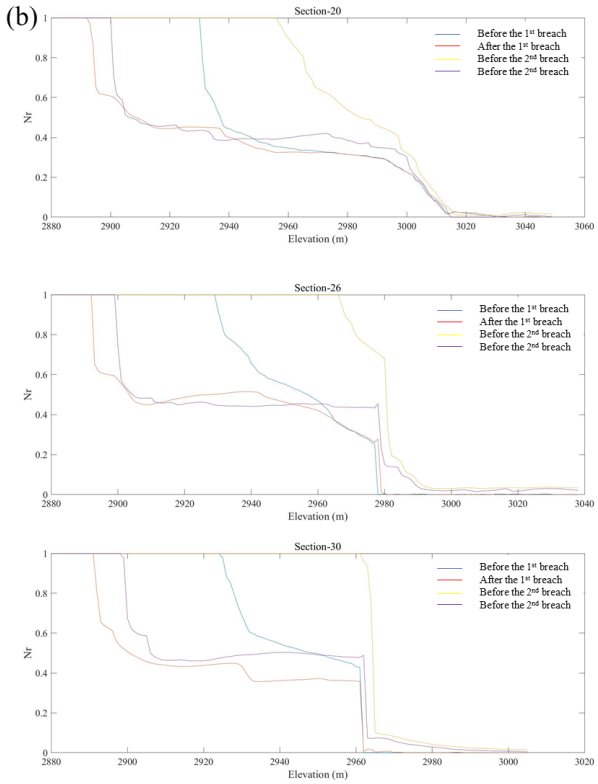

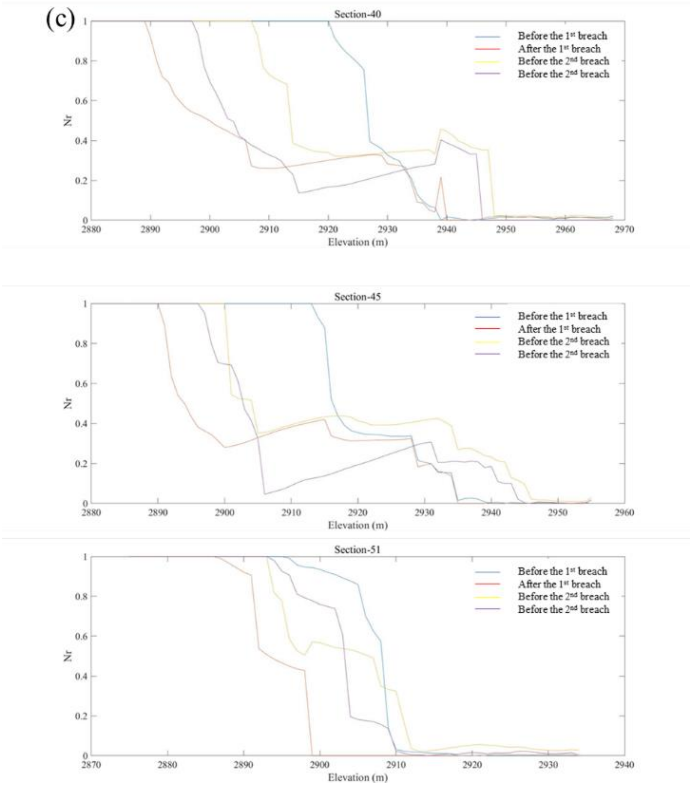

Fig.A5. Analysed *N*r values for three different areas: a) upstream area; b) middle area; c) downstream area.

Nomenclature

a, b and k: coefficients of erosion model

AV_n: accumulated dam volume in the river (m^3)

A: the water surface area, which: considered as a function of elevation H (m^2)

ACR, *R*, *DCI*, and *DMI*: judging coefficients

B_c: channel width (m)

B_r: river width (m)

B_D: dam width (m)

B_L: landslide width (across valley) (m)

$B(H)$: the breach width at elevation H (m)

C: discharge coefficient

d: the average particle diameter of soil sample (m)

DV_n: the volume of the n^{th} dam (m^3)

g: gravitational acceleration (m/s^2)

h_T: highest water level before dam breach (m)

h_{avg}: average depth of dam (m)

h_r: river flow depth (m)

h_L: landslide depth (thickness) (m)

685 h: flow depth (m)

686 H_s: elevation of the spillway base after dam breach (m)

687 H_B: effective height of old breach (m)

688 H_N: dam height variation based on breached new geometry (m)

689 H_R: dam height where there is no old blocking condition (m)

690 H_{en}: effective height of the new dam (m)

691 H_e: effective dam height (m)

692 K: a coefficient for mixed sand

693 L_D: dam length along river (m)

694 LV: lake volume (m)

695 $N_r(H)$: the narrowing ratio at elevation H *(m)*

696 n: the roughness coefficient ($m^{-1/3}$·s)

697 PE: potential energy of the barrier lake (J)

698 Q_{P_5}: 5 year return period discharge (m^3/s)

699 Q_p: peak discharge (m^3/s)

700 Q: spillway discharge (m^3/s)

701 q: the natural inflow to the landslide barrier lake *(*m^3/s*)*

702 Q_b: base flow rate of river (m^3/s)

703 q_w: upstream inflow rate per unit width (m^3/s)

704 R': the hydraulic radius (m)

705 $R(H)$: the initial river width at elevation *H (m)*

706 $\bar{V}$: average velocity of the landslide (m/s)

707 V_{ML}: maximum lake volume (m^3)

708 V_L: landslide volume (m^3)

709 V_D: dam volume (m^3)

710 V_1: the volume of first landslide dam (m^3)

711 Z: the elevation of the spillway base (m)

712 θ: river slope (m)

713 γ: the specific weight of water (N/m^3)

714 γ_s*:* the unit weight of dam material, (N/m^3)

715 ρ_s: landslide bulk density (kg/m^3)

716 ρ_w: water density (kg/m^3)

717 ΔE: elevation difference in one mesh, (m)

718 ΔH: the difference of dam height between blocking and no blocking condition (m)

719 $\frac{\Delta Z}{\Delta t}$: erosion rate of the spillway (m/s)

720 τ: bottom shear stress (Pa)

721 τ_c: critical shear stress (Pa)

722

723 ## Reference

724 Al-Riffai, M., 2014. Experimental study of breach mechanics in overtopped noncohesive earthen
725 embankments. PhD thesis, University of Ottawa.

726 Bazai, NA, Cui P, Carling PA, Wang H, Hassan J, Liu D, Zhang G, Jin W, 2021. Increasing glacial
727 lake outburst flood hazard in response to surge glaciers in the Karakoram. Earth-Science
728 Reviews 212, 103432. doi:https://doi.org/10.1016/j.earscirev.2020.103432.

729 Begam, S., Sen, D., Dey, S., 2018. Moraine dam breach and glacial lake outburst flood generation
730 by physical and numerical models. J. Hydrol. 563, 694-710.

731 Bohorquez, P., Cañada-Pereira, P., Jimenez-Ruiz, P.J., del Moral-Erencia, J.D., 2019. The
732 fascination of a shallow-water theory for the formation of megaflood-scale dunes and antidunes.
733 Earth Sci. Rev. 193, 91-108.

734 Briaud, J., Ting, F.C.K., Chen, H., Cao, Y., Han, S.W., Kwak, K., 2001. Erosion Function Apparatus
735 for Scour Rate Predictions. J. Geotech. Geoenviron. 127 (2), 105-113.

736 Burr, D.M., Carling, P.A., Baker, V.R., 2009. Megaflooding on Earth and Mars. Cambridge
737 University Press.

738 Cantelli, A., Wong, M., Parker, G., Paola, C., 2007. Numerical model linking bed and bank evolution
739 of incisional channel created by dam removal. Water Resour. Res. 43 (7), 931-936.

740 Cao, Z., Yue, Z., Pender, G., 2011. Landslide dam failure and flood hydraulics. Part II: coupled
741 mathematical modelling. Nat. Hazards. 59 (2), 1021-1045.

742 Capps, D.M., Clague, J.J., 2014. Evolution of glacier-dammed lakes through space and time; Brady
743 Glacier, Alaska, USA. Geomorphology 210, 59-70.

744 Carling, P., Villanueva, I., Herget, J., Wright, N., Borodavko, P., Morvan, H., 2010. Unsteady 1D
745 and 2D hydraulic models with ice dam break for Quaternary megaflood, Altai Mountains,
746 southern Siberia. Global. Planet. Change. 70 (1), 24-34.

747 Carling, P.A., Fan, X., 2020. Particle comminution defines megaflood and superflood energetics.
748 Earth Sci. Rev. 204, 103087.

749 Carling, P.A., 2013. Freshwater megaflood sedimentation: What can we learn about generic
750 processes? Earth Sci. Rev. 125, 87-113.

751 Chang, D.S., Zhang, L.M., 2010. Simulation of the erosion process of landslide dams due to
752 overtopping considering variations in soil erodibility along depth. Nat. Hazard. Earth. Sys. 10
753 (4), 933-946.

754 Chang, D.S., Zhang, L.M., Xu, Y., Huang, R.Q., 2011. Field testing of erodibility of two landslide
755 dams triggered by the 12 May Wenchuan earthquake. Landslides 8 (3), 321-332.

Chen, C., Zhang, L., Xiao, T., He, J., 2020. Barrier lake bursting and flood routing in the Yarlung Tsangpo Grand Canyon in October 2018. J. Hydrol. 583, 124603.

Chen, J., Cui, Z.J., University, B., 2015. Discovery of Outburst Deposits Induced by the Xuelongnang Paleolandslide-Dammed Lake in the Upper Jinsha River, China and Its Environmental and Hazard Significance. Acta Sedimentologica Sinica. 2(33), 275-284. (in chinese)

Chen, Z., Ma, L., Yu, S., Chen, S., Zhou, X., Sun, P., Li, X., 2014. Back analysis of the draining process of the Tangjiashan barrier lake. J. Hydraul. Eng. 141 (4), 05014011.

Choi, C, Cui, Y.F., Au, K., Liu, H.M., Wang, J., Liu, D.Z., Wang, H., 2018. Case Study: Effects of a Partial-Debris Dam on Riverbank Erosion in the Parlung Tsangpo River, China. Water 2018, 10 (3), 250.

Cook, S.J., Kougkoulos, I., Edwards, L.A., Dortch, J.M., Hoffmann, D., 2016. Glacier change and glacial lake outburst flood risk in the Bolivian Andes. The Cryosphere 10 (5), 2399-2413.

Costa, J.E., Schuster, R.L., 1988. The formation and failure of natural dams. Geol. Soc. Am. Bull. 100 (7), 1054-1068.

Cui, P., Dang, C., Zhuang, J.Q., You, Y., Chen, X.Q., Scott, K.M., 2012. Landslide-dammed lake at Tangjiashan, Sichuan province, China (triggered by the Wenchuan Earthquake, May 12, 2008): risk assessment, mitigation strategy, and lessons learned. Environ. Earth. Sci. 65 (4), 1055-1065.

Cui, P., Zhu, Y.Y., Han, Y.S., Chen, X.Q., Zhuang, J.Q., 2009. The 12 May Wenchuan earthquake-induced landslide lakes: distribution and preliminary risk evaluation. Landslides 6 (3), 209-223.

Del Sasso, S.F., Sole, A., Pascale, S., Sdao, F., Bateman Pinzón, A., de Medina Iglesias, V.C., 2014. Assessment methodology for the prediction of landslide dam hazard. Nat. Hazard. Earth. Sys. 14 (3), 557-567.

Entwistle, N.S., Heritage, G.L., 2019. Small unmanned aerial model accuracy for photogram metrical fluvial bathymetric survey. J. Appl. Remote. Sens. 13, 014523.

Entwistle, N.S.; Heritage, G., 2017. An evaluation DEM accuracy acquired using a small unmanned aerial vehicle across a riverine environment. Int. J. New Technol. Res. 3, 43–48.

Ermini, L., Catani, F., Casagli, N., 2005. Artificial Neural Networks applied to landslide susceptibility assessment. Geomorphology, 66(1/4), 327-343.

Fan, X., Scaringi, G., Korup, O., West, A.J., Westen, C.J., Tanyas, H., Hovius, N., Hales, T.C., Jibson, R.W., Allstadt, K.E., Zhang, L., Evans, S.G., Xu, C., Li, G., Pei, X., Xu, Q., Huang, R., 2019a. Earthquake‐Induced Chains of Geologic Hazards: Patterns, Mechanisms, and Impacts. Rev. Geophys. 57 (2), 421-503.

Fan, X., Xu, Q., Alonsorodriguez, A., Subramanian, S.S., Li, W., Zheng, G., Dong, X., Huang, R., 2019b. Successive landsliding and damming of the Jinsha River in eastern Tibet, China: prime investigation, early warning, and emergency response. Landslides 16 (5), 1003-1020.

794 Fread, D.L., 1988. BREACH, an erosion model for earthen dam failures, Hydrologic Research
795 Laboratory, National Weather Service, NOAA.

796 Garcia-Castellanos, D., Estrada, F., Jimenez-Munt, I., Gorini, C., Fernandez, M., Verges, J., De
797 Vicente, R., 2009. Catastrophic flood of the Mediterranean after the Messinian salinity crisis.
798 Nature 462 (7274), 778-781.

799 George, D.L., Iverson, R.M., Cannon, C.M., 2017. New methodology for computing tsunami
800 generation by subaerial landslides: Application to the 2015 Tyndall Glacier landslide, Alaska.
801 Geophys. Res. Lett. 44 (14), 7276-7284.

802 Hanson, G.J., Simon, A., 2001. Erodibility of cohesive streambeds in the loess area of the
803 midwestern USA. Hydrol. Processes 15 (1), 23-38.

804 Hu, K.H., Zhang, X., You, Y., Hu, X.D., Liu, W.M., Li, Y., 2019. Landslides and dammed lakes
805 triggered by the 2017 Ms6.9 Milin earthquake in the Tsangpo gorge. Landslides 16 (5), 993-
806 1001.

807 Jiang, X.G., Huang, J.H., Wei, Y.W., Niu, Z.P., Chen, F.H., Zou, Z.Y., Zhu Z.Y., 2018. The influence
808 of materials on the breaching process of natural dams. Landslides. 2018, 15 (2), 243-255.

809 Korup, O., Strom, A., Weidinger, J.T., 2006. Fluvial response to large rock-slope failures: Examples
810 from the Himalayas, the Tien Shan, and the Southern Alps in New Zealand. Geomorphology
811 78 (1), 3-21.

812 Korup, O., Tweed, F.S., 2007. Ice, moraine, and landslide dams in mountainous terrain. Quat. Sci.
813 Rev. 26 (25), 3406-3422.

814 Korup, O., Montgomery, D.R., 2008. Tibetan plateau river incision inhibited by glacial stabilization
815 of the Tsangpo gorge. Nature 455 (7214), 786-789.

816 Lang, K.A., Huntington, K.W., Montgomery, D.R., 2013. Erosion of the Tsangpo Gorge by
817 megafloods, Eastern Himalaya. Geology 41 (9), 1003-1006.

818 Larsen, I.J., Lamb, M.P., 2016. Progressive incision of the Channeled Scablands by outburst floods.
819 Nature 538 (7624), 229-232.

820 Li, B., Feng, Z., Wang, G., Wang, W., 2016. Processes and behaviors of block topple avalanches
821 resulting from carbonate slope failures due to underground mining. Environ. Earth. Sci. 75 (8),
822 694.

823 Liao, H.M., Yang, X.G., Lu, G.D., Tao, J., Zhou, J.W., 2019. Experimental study on the formation
824 of landslide dams by fragmentary materials from successive rock slides. Bull. Eng. Geol.
825 Environ 79, 1591-1604.

826 Liu, N., Chen, Z., Zhang, J.X., Lin, W., Chen, W., Xu, W.J. 2010. Draining the Tangjiashan
827 barrier lake. J. Hydraul. Eng. 136(11), 914-923.

828 Liu, W.M., Carling, P.A., Hu, K.H., Wang, H., Zhou, Z., Zhou, L.Q., Liu, D.Z., Lai, Z.P., Zhang,
829 X.B., 2019. Outburst floods in China: A review. Earth Sci. Rev. 197, 102895.

830 Ma, D.T., 2006. Study on Influences of Mountain Hazards in Yigong Zangbu River Basin to
831 Mitigation and Reconstruction of Sichuan-Tibetan Highway Line. PhD thesis, The Graduate

School of Chinese Academy of Sciences (in chinese).

Niu, Z.P., Wei-Lin, X.U., Nai-Wen, L.I., Yang, X., Chen, H.Y., 2012. Experimental investigation of the failure of cascade landslides dams (in chinese). Journal of Hydrodynamics. 24 (3), 430-441.

Osman, A.M., Thorne, C.R., 1988. Riverbank Stability Analysis. I: Theory. J. Hydraul. Eng. 114 (2), 134-150.

Ouyang, C., An, H., Zhou, S., Wang, Z., Su, P., Wang, D., Cheng, D., She, J., 2019. Insights from the failure and dynamic characteristics of two sequential landslides at Baige village along the Jinsha River, China. Landslides (4), 1-18.

Owen, L.A., 2008. Geomorphology: How Tibet might keep its edge. Nature 455 (7214), 748-749.

Peng, M., 2012. Breaching parameters of landslide dams. Landslides 9 (1), 13-31.

Samia, J., Temme, A.J.A.M., Bregt, A.K., Wallinga, J., Guzzetti, F., Ardizzone, F., Rossi, M., 2017. Characterization and quantification of path dependency in landslide susceptibility. Geomorphology 292, 16-24.

Schuster, R. L., 2006. Impacts of landslide dams on mountain valley morphology. Landslides 49, 591-616.

Singh, V.P., 2013. Dam breach modeling technology. Springer Science & Business Media.

Song, L. 2015. Landslide damming in Western Sichuan Province, China. Master thesis, University of Waterloo.

Swanson, F. J., Graham, R. L., Grant, G. E., 1985. Some effects of slope movements on river channel. Proceedings of the International Symposium on Erosion, Debris Flow and Disaster Prevention, Tsukuba, Japan, 273-278.

Swartenbroekx, C., Zech, Y., Soares-Frazão, S., 2013. Two-dimensional two-layer shallow water model for dam break flows with significant bed load transport. Int. J. Numer. Methods Fluids 73 (5), 477-508.

Teller, J.T., Leverington, D.W., Mann, J.D., 2002. Freshwater outbursts to the oceans from glacial Lake Agassiz and their role in climate change during the last deglaciation. Quat. Sci. Rev. 21 (8-9), 879-887.

Tonkin, T. Midgley, N., 2016 Ground-control networks for image-based surface reconstruction: An investigation of optimum survey designs using UAV derived imagery and structure-from-motion photogrammetry. Remote Sens. 8(9), 786-786.

Turzewski, M.D., Huntington, K.W., LeVeque, R.J., 2019. The Geomorphic Impact of Outburst Floods: Integrating Observations and Numerical Simulations of the 2000 Yigong Flood, Eastern Himalaya. J. Geophys. Res-Earth. 124(5), 1056-1079.

Walder, J.S., Iverson, R.M., Godt, J.W., Logan, M. , Solovitz, S.A., 2015. Controls on the breach geometry and flood hydrograph during overtopping of noncohesive earthen dams. Water Resour. Res. 51(8), 6701-6724.

Wang, G.Q., Liu, F., Fu, X.D., Li, T.J., 2008. Simulation of dam breach development for emergency

869 treatment of the Tangjiashan Quake Lake in China. Science in China 51 (2), 82-94.

870 Wang, H., Cui, P., Liu, D., Liu, W., Bazai, N.A., Wang, J., Zhang, G., Lei, Y., 2019. Evolution of a
871 landslide-dammed lake on the southeastern Tibetan Plateau and its influence on river
872 longitudinal profiles. Geomorphology 343, 15-32.

873 Wang, L., Chen, Z., Wang, N., Sun, P., Yu, S., Li, S., Du, X., 2016. Modeling lateral enlargement in
874 dam breaches using slope stability analysis based on circular slip mode. Eng. Geol. 209, 70-
875 81.

876 Wei, L., Chen, J., Wang, P.F., Xv, C., Liu, H., Sun, J.Z., 2015. Formation Mechanism and Back
877 Analysis of Paleoseismic Parameters of the Temi Large-scale Ancient Landslide in the Upper
878 Jinsha River (in chinese). Journal of Seismological Research 38 (4), 568-575.

879 Wei, R., Zeng, Q., Davies, T., Yuan, G., Wang, K., Xue, X., Yin, Q., 2018. Geohazard cascade and
880 mechanism of large debris flows in Tianmo gully, SE Tibetan Plateau and implications to
881 hazard monitoring. Eng. Geol. 233, 172-182.

882 Wei, X., Huang, X., Pan, L., Zhang, L. 2019. Response of Runoff Change to Climate in the Upper
883 Reaches of Jinsha River in Past 60 Years (in chinese). Water Power 45 (8), 12-17.

884 Wu, H., Nian, T.K., Chen, G.Q., Zhao, W., Li, D.Y., 2020. Laboratory-scale investigation of the 3-
885 D geometry of landslide dams in a U-shaped valley. Eng. Geol. 265, 105428.

886 Yan, Y., Cui, Y.F., Guo, J., Hu, S., Yin, S.Y., 2020. Landslide reconstruction using seismic signal
887 characteristics and numerical simulations: Case study of the 2017 "6.24" Xinmo landslide. Eng.
888 Geol. 270, 105582.

889 Zhang, L., Xiao, T., He, J., Chen, C., 2019. Erosion-based analysis of breaching of Baige landslide
890 dams on the Jinsha River, China, in 2018. Landslides 16 (10), 1965-1979.

891 Zhong, Q., Chen, S., Wang, L. and Shan, Y., 2020. Back analysis of breaching process of Baige
892 landslide dam. Landslides 17, 1681-1692.

893 Zhou, J., Cui, P., Hao, M., 2016. Comprehensive analyses of the initiation and entrainment processes
894 of the 2000 Yigong catastrophic landslide in Tibet, China. Landslides 13 (1), 39-54.

895 Zhou, X., Chen, Z., Li, S.Y., Wang, L., 2015. Comparison of Sediment Transport Model in Dam

896 Break Simulation. Journal of basic science and engineering 23(6), 1097-1108 (in chinese)